



This is to certify that the

dissertation entitled

Evaluation of Multi-Layered Material Properties
By Acoustic Reflectrometry

presented by

Tainsong Chen

has been accepted towards fulfillment of the requirements for

Ph.D. degree in Electrical Engr

Date 6/11/9/

MSU is an Affirmative Action/Equal Opportunity Institution

0-12771

### LIBRARY Michigan State University

PLACE IN RETURN BOX to remove this checkout from your record. TO AVOID FINES return on or before date due.

DATE DUE	DATE DUE	DATE DUE

MSU Is An Affirmative Action/Equal Opportunity Institution c:tc/rc/datedua.pm3-p.1

# Evaluation of Multi-layered Material Properties from Acoustic Reflectometry

By
Tainsong Chen

#### **A DISSERTATION**

Submitted to

Michigan State University in partial fulfillment of requirements for the degree of

**DOCTOR OF PHILOSOPHY** 

Department of Electrical Engineering 1991

654-626

#### **ABSTRACT**

# EVALUATION OF MULTI-LAYERED MATERIAL PROPERTIES BY ACOUSTIC REFLECTOMETRY

BY

#### Tainsong Chen

This dissertation consists of two parts. One part presents a time domain technique to evaluate multi-layered material properties (attenuation coefficients and acoustic impedances) by a two sided interrogation configuration. The second part employs the spectral shift method to measure the multi-layered material properties (attenuation coefficients and acoustic impedances) by a single sided interrogation.

The time domain approach utilizes transducers applied to both sides of the target to measure the attenuation coefficient and the acoustic impedance for individual layers under the assumption of a narrow-band incident wave. This method is developed based solely on peak amplitude ratios of the successive time domain echo returns from both sides of the target. We can determine the attenuation coefficient and acoustic impedance from the impulse response of the target. The results of a five-layer experimental model are compared with the reference values determined by a single layer measurement for checking the validity of the approach.

The spectral shift method requires that the propagating pulse has a Gaussian-shaped spectrum, and the transfer function of each layer be characterized by either linear or quadratic frequency dependent attenuation. Since this method does not require information on

#### Tainsong Chen

the reflection coefficients to determine the attenuation coefficient, we can determine the attenuation coefficient and acoustic impedance for each layer by a single sided interrogation. This method derives the attenuation coefficients and acoustic impedances for individual layers from the information of down-shifted center frequency and spectral amplitude peak ratios of successive gated pulses. Experimental results for a three-layer model are compared to the published data to confirm the validity of the approach.

#### **ACKNOWLEDGEMENTS**

I would like to thank my advisors, Professors B. Ho. and R. Zapp, for their constant guidance, encouragement, valuable suggestions and inspiring discussions throughout the course of this study.

Thanks also are given to the guidance committee members, Professors J. Deller and D. Yen for taking time to serve on the examining committee.

Finally, the support from my parents and my wife, Peggy, during this study are greatly appreciated.

#### TABLE OF CONTENTS

LIST OF FIGURES	
Chapter I INTRODUCTION	1
I.1 Applications of ultrasonic imaging	1
I.2 Parameters of ultrasonic imaging	2
I.3 Research objective	5
I.4 Thesis organization	7
Chapter II BACKGROUND	9
II.1 Basic wave equations and some acoustic terminology	9
II.2 Reflection and transmission of acoustic wave at	
a normal to the boundary	12
II.3 Wave propagation with attenuation	16
Chapter III TIME DOMAIN ANALYSIS FOR MULTI-LAYERED	
MATERIAL	21
III.1 Limitations and advantages of time domain techniques	21
III.2 Evaluation of multi-layered material properties by	
time domain techniques	24
III.3 Accuracy of time domain techniques for attenuation measurement	33
Chapter IV FREQUENCY DOMAIN ANALYSIS FOR	
MULTI-LAYERED MATERIAL	41
IV.1 Comparison of the spectral shift and spectral difference methods	41
IV.2 Evaluation of multi-layered material properties by	
spectral shift techniques	44
IV.3 Evaluation of nonlinear attenuation parameters	56
Chapter V EXPERIMENTAL SETUP AND RESULTS	62
V.1 Time domain methods for material properties evaluation	62
V.2 Spectral shift methods for material properties evaluation	76

Chapter VI SUMMARY AND CONCLUSIONS	
VI.1 Limitations and advantages of the proposed time	
domain method.	89
VI.2 Limitations and advantages of the proposed spectral	
shift method.	90
BIBLIOGRAPHY	93

#### **LIST OF FIGURES**

Figure II.1 Normal incident wave at interface between two different media	
with different acoustic impedance.	13
Figure II.2 The ultrasonic wave propagating through multi-layered material	
affected by reflection coefficient and attenuation under a narrow	
band incident signal assumption.	19
Figure II.3 The wave propagating through multi-layered structure described	
in frequency domain.	20
Figure III.1 Dual pulse-echo interrogation of a layered structure.	25
Figure III.2 Impulse response of dual interrogation configuration.	28
Figure III.3 Experimental setup for measuring r <sub>1</sub> , (a) configuration for	
reference, (b) obtaining echo from first boundary.	31
Figure III.4 Time and frequency domain representation of the incident signal.	35
Figure III.5 The theoretical peak amplitude error of the interrogating wave	
passing through 2.0 cm and 1.0 cm plexiglass.	40
Figure IV.1 Multi-layered medium model.	45
Figure IV.2 Reflected signal gating by a variable window to obtain	
a sequence of pulses.	48
Figure IV.3 The downshift in center frequency and amplitude reduction	
for sequential gated pulses.	51
Figure IV.4 Schematic for measuring the first reflection coefficient.	<b>5</b> 3
Figure IV.5 The deviation of the approximation for different exponent dependency.	58
Figure V.1 Schematic for the experimental setup for time domain measurements.	67
Figure V.2 Measured pulse echoes for dual interrogation.	68
Figure V.3 Impulse responses of two sided interrogation.	69
Figure V.4 Schematic for measuring sample properties.	70
Figure V.5 The captured signals from Figure V.4 setup.	71
Figure V.6 Attenuation profiles of multi-layered model by time domain techniques.	72
Figure V.7 Acoustic impedance profiles of multi-layered model by	
time domain techniques.	73

### viii

Figure V.8 Acoustic velocity profiles of multi-layered model by	
time domain techniques.	74
Figure V.9 Attenuation-velocity product profiles of multi-layered model	
by time domain techniques.	75
Figure V.10 Schematic for multi-layered target measurements.	80
Figure V.11 The captured signals from a one sided multi-layered model.	81
Figure V.12 Measured sequence of gated pulses by variable windows.	82
Figure V.13 Zero padding of the gated pulses to generate 1024-point signals.	83
Figure V.14 The spectral amplitudes of the gated pulses on a linear scale.	85
Figure V.15 Normalized spectral magnitudes of the gated pulses on a	
linear scale.	86
Figure V.16 Attenuation coefficient profiles of multi-layered model obtained	
by spectral shift techniques.	87
Figure V.17 Acoustic impedance profiles of multi-layered model obtained	
by spectral shift techniques.	88

## **CHAPTER I**

#### INTRODUCTION

#### I.1. Applications of ultrasonic imaging

Pulsed-echo ultrasound is an important and valuable tool in nondestructive evaluation (NDE) of material and noninvasive clinical applications. It employs high frequency mechanical wave propagation and interaction with the objective of deriving information on internal structure. The ultrasonic imaging system has provided valuable clinical diagnostic information with no apparent harm to the patient or the operator. Therefore much effort has gone into improving the diagnostic significance of an ultrasonic examination with the concentration on improving the quality of the resulting images. X-ray computerized tomography (CT) utilizes the narrow beam X-ray to get images of specific tissue, where the X-ray interaction is proportional to the density of the tissue. Therefore, injection of a contrast medium (such as iodine) for visualization of nonbony tissue is necessary and the procedure is no longer noninvasive. The nuclear magnetic resonance (NMR) techniques, which measure the selective resonances of radioactive isotopes in particular organs and thus provide information concerning organ function, provide a third form of significant

medical imaging diagnosis. Although ultrasonic imaging systems unlike X-ray tomography and nuclear magnetic resonance imaging systems which provide excellent pictures of internal structure, yield unclear images the lower cost and a good differentiation of soft tissue by noninvasive techniques continue to favor ultrasound for material property evaluation.

#### L2 Parameters of ultrasonic imaging

Differences in the acoustic impedance, attenuation and sound speed of various normal and abnormal tissue were studied under a variety of known and controlled ultrasonic field conditions. These were found to be quantitatively significant and could be correlated with differences in tissue structure and pathological changes. In the past two decades, there were many techniques proposed for estimating these quantities. Attenuation has been considered an important tissue characteristic capable of forming the basis for a tissue differentiation scheme [1]. Attenuation estimation has progressed from specifically transmission techniques to the more clinically acceptable backscattering methods. The transmission methods [2-3,6] are conceptually simple and straightforward. However, these approaches are limited to in vitro measurements so that few human organs can be accessed (such as woman's breasts). For example, transmission computer-assisted tomography has been used to estimate attenuation in lesions and normal breast tissue [3-6]. Attenuation estimation in the reflection mode was developed by Kuc et al. [7-10]. This method is a modification of the transmission substitution method under the assumptions that the attenuation coefficient is proportional to the frequency. Under this assumption the Gaussian frequency spectrum of the interrogating wave yields an echo whose Gaussian mean spectrum is downshifted. The attenuation coefficient is estimated by comparison to the normalized spectrum. A number of methods for estimating attenuation coefficients from the reflected signals have been

proposed including both time domain and frequency domain techniques. The time domain method extracts the attenuation information from A-mode signals [11-16], while the frequency domain method employs the spectral shift or spectral difference from broadband signals for estimating the deviation of the mean log spectrum of backscattering echoes [10]. Time domain methods encounter the difficulties in resolving consecutive echoes from thin layers due to echo overlap, and in identifying pulses from highly dispersive media, due to pulse shape distortion. To avoid the pulse distortion, a narrow band spectrum for the interrogating pulse should be assumed. However, a narrowband incident pulse will result in reduced range resolution. In addition, a narrow-band signal pulse is very difficult to realize in conventional ultrasonic systems. Therefore, if the bandwidth of the ultrasonic signal is very large and the frequency shift due to material attenuation is significant, the time domain method might produce a biased estimate. P. He [11,16] proposed a modified envelope peak (EP) method by pre-processing the wideband echo signal using a split spectrum technique [17-23] to obtain a bank of narrow-band signals which were used to estimate the attenuation by narrow-band approaches. The split spectrum technique was used by Newhouse et al. [19,21,23] to improve signal-to-noise ratio (SNR) in ultrasonic flaw detection and used by Gehlbach et al. [22] to increase SNR in B-scan images. For overlapping echoes a number of deconvolution schemes have been proposed to improve range resolution [24-27], or lateral resolution [28-29]. The received signals deconvolved with the incident signal are used to obtain the impulse response of the test object. The impulse response of the test object contains information about the attenuation and the reflection coefficient as well. The overlapped signals in the time domain can be resolved two boundaries by separating locations of peaks of the impulse response. For the cases, where frequency dependent attenuation is not linear or quadratic, a closed form impulse response is not possible. Thus, it becomes impossible to obtain the attenuation coefficient from the impulse response. In spite of these limitations, the time domain technique provides an excellent possibility of real-time imaging because of its short processing.

The acoustic impedance is an important quantity for evaluating mineral and biological resources. J. P. Jones [30] utilized the returning echoes deconvolved with the transmitted wave to produce the impulse response in which yields impedance as function of time under the assumption of the wave propagating through non-attenuating media. Finally, he set up an experiment to determine the impedance profile of multi-layered biological tissue. Parra and Guerra [31] determined the impedance profile of a multi-layered ocean floor. However, their technique required complicated processing for impulse deconvolution; and their treatment of attenuation is overly simplified by the hypothesis of linear frequency-dependency and the same acoustic thickness for each layer. In this dissertation, we will relax these assumptions in the theoretical development.

The speed of sound propagation in tissue is an important physical property of material. Kossoff et al. [32,42] demonstrates that this parameter correlates with some pathological characteristic of tissue. However, the propagation velocity has not been extensively utilized in medical diagnosis to date, because, the pathology related changes in the speed of sound are on the order of several percent, and measurement of sound speed in vivo is difficult. Greenleaf et al. [4-5] used transmission techniques and time-of-flight (TOF) tomography to produce two dimensional sound speed images of female breast tissue. In practice, the speed of sound can be measured using transmission [33-38] or by using pulse echo methods [39-41]. Simple transmission techniques in general measure the transit time of the primary sound pulse as it passes through different layers which could have different sound speed, thus a particular layer may not be identified. Thus, even with an accurate transit time measurement the precise material thickness is required to determine the sound speeds. However, the material thickness is not available in most experimental configurations. Another problem results from the ultrasonic pulse passing through frequency dependent attenuating media resulting in pulse distortion which complicate the estimate for transit time based on peak pulse locations.

#### I.3 Research objective

Evaluation of multi-layered material properties (attenuations and acoustic impedances) by pulsed-echo ultrasound is very useful in the areas of geoacoustic exploration, material evaluation and biomedical studies. An ultrasound signal reflected from internal discontinuity contains not only information about the reflection coefficients at each discontinuity, but also the attenuation of the medium between each boundary [43]. It is almost impossible to separate backscatter and attenuation by using a single pulse echo return in the time domain. J. P. Jones [30] derived the acoustic impedance profile of multi-layered structures under the assumptions of equal reflection coefficients at each boundary for non-attenuating media. These two assumptions are rather restrictive and not practical for modeling a multi-layered structure. Parra and Guerra [31] determined the impedance profile and estimated the overall attenuation of a multi-layered ocean floor. Their approach requires complicated processing for impulse response deconvolution and assumes equal acoustic thickness. Moreover, their treatment of attenuation is overly simplified by the hypothesis of linear frequency-dependency of each layer. Dines and Kak [2] utilized the spectral-shift and transmission substitution method to estimate the overall attenuation for multi-layered tissue. None of the above mentioned methods can evaluate both attenuation and acoustic impedance for individual layers. A dual pulse echo technique proposed by B. Ho et al. [44], and modified by T. Chen et al. [45] to evaluate material properties of multi-layered structures, in which a narrow-band incident signal approximation is used to interrogate the multi-layered structures. If the attenuation remains constant within the bandwidth of the incident wave, then the total stress wave will travel undistorted through the medium. Under this condition the attenuation coefficients and acoustic impedances can be evaluated by using echo returns from both sides of the target. However, a narrow-band assumption is very difficult to realize in conventional ultrasonic systems. For frequency dependent ultrasonic attenuation, the individual frequency components of an acoustic pulse will be attenuated by different degrees, resulting in pulse shape distortion. The diminution in pulse amplitude with distance will not follow the commonly assumed exponential law, such as  $exp(-\beta f_c^n D)$ , where  $\beta$  is the attenuation coefficient,  $f_c$  is the center frequency of the incident pulse and D is the distance traveled. The deviation from exponential form is a function of pulse width, attenuation and distance traveled [46].

In general, frequency domain techniques can be broadly divided into spectral difference and spectral shift approaches [47-51]. The spectral difference method [52-53] estimates the attenuation,  $\alpha(f) = \beta_0 f^n$ , by curve fitting from the information of spectral difference. Thus, no specific spectral form of the incident pulse is required to estimate the parameters  $\beta_0$  and n, where n is not restricted to be an integer. However, the spectral difference between the input and output signals contains both the attenuation and reflection coefficient parameters. They could not be determined by simply using the signal information of a single trace of the echo return. In order to obtain meaningful results, one can either ignore the effect of reflection coefficient [8-9] or assume it to be a known quantity [2]. In reality, the reflection coefficient does exist at an interface and is an important factor governing the reduction in spectral power of the reflected signals. When a multi-layered structure is considered, the strength of the echo return is heavily dependent on the reflection coefficient of successive layer interfaces. Therefore, in the research reported here we will take the reflection coefficients into account as well.

The spectral shift techniques for ultrasound propagation through frequency-dependent media was originally suggested by Serabian [47]. Kuc [7-9] applied this concept to evaluate attenuation coefficients in linear frequency-dependent soft tissue. Dines and Kak [2] employed the technique to measure the overall attenuation of multi-layered tissue. J. Ophir *et al.* [51] extended the method to nonlinear frequency-dependent media. The spectral shift approach requires a Gaussian-shaped spectrum for the incident pulse. However, it

does not require knowledge of the reflection or transmittance for estimating the attenuation. As a result, one can obtain both attenuation and acoustic impedance for individual layers from single sided interrogation alone, which is easier to carry out experimentally than two sided interrogation.

In summary, the objectives of this dissertation are:

- 1. Determination of multi-layered material properties (attenuation and acoustic impedance).
- 2. Under a narrow-band assumption, to utilize a two-sided interrogation to provide a simple resolution of attenuation and impedance.
- To determine multi-layered material properties with a linearly frequency-dependent attenuation and quadratic frequency-dependent attenuation model and a single sided interrogation.
- 4. To extend the attenuation parameter n to the range 1 < n < 2.

#### I.4 Thesis organization

The organization of this dissertation is as follows: In chapter II, some background material is presented. Section II.1 shows the basic wave behavior and some acoustic terminology. This includes solution of the one dimensional wave equation, definition of acoustic impedance and determination of ultrasonic intensity. Section II.2 defines and derives the reflection and transmission coefficients and derives them in terms of pressure amplitude and power. Section II.3 builds up the wave propagation model in the time domain and in the frequency domain, respectively. Evaluation of multi-layered material properties by time domain techniques is presented in chapter III. The limitations and advantages of time domain approaches are pointed out in section III.1, and it provided a review of some

existing time domain approaches. The theroretical development of the time domain method to investigate multi-layered material under a narrowband assumption is derived in section III.2. The deviation from a narrow-band assumption is discussed in section III.3. Evaluation of multi-layered material properties by spectral shift techniques is presented in chapter IV. Some existing frequency domain approaches are reviewed and compared in section IV.1. This includes a comparison of advantages and disadvantages of the spectral difference and spectral shift methods. Section IV.2 fomulates relationships between the downshifted center frequency and attenuation coefficients and the spectral amplitudes and acoustic impedance. The attenuation parameter n extended to 1 < n < 2, is formulated in section IV.3. This includes the closed form for attenuation coefficient and for the exponent frequency dependency. The experimental setup and results for the time domain technique and for the spectral shift technique are shown in chapter V. Finally, some conclusions and suggested future research is provided in chapter VI.

# **CHAPTER II**

#### **BACKGROUND**

#### II.1 Basic wave behavior and some acoustic terminology

The ultrasonic wave parameters are pressure, particle displacement and density. Unlike electromagnetic waves, sound waves require a medium through which to travel. If the driving source produces particle displacement in the propagation direction, the wave is called a compressional or longitudinal wave; if it produces displacement perpendicular to the propagation direction it is called a shear or transverse wave. Ultrasonic waves used in medical and material evaluation applications are longitudinal. Therefore, only longitudinal waves are considered in this dissertation. In order to simplify the analysis, we consider an one-dimensional plane longitudinal wave. Mechanical waves that propagate through media, have a behavior that is governed by the following equations:

$$\frac{\partial^{2} \Phi(x,t)}{\partial t^{2}} \Phi(x,t) = c^{2} \cdot \frac{\partial^{2} \Phi(x,t)}{\partial x^{2}} \Phi(x,t)$$
 (II.1.1)

where  $\Phi(x,t)$  is the acoustic field and c is the propagation speed of sound.

The acoustic field  $\Phi(x,t)$  in equation(II.1.1) has the general solution:

$$\Phi(x,t) = Ae^{i(\omega t \pm kx)}$$
 (II.1.2)

where A is amplitude,  $\omega$  is radian frequency, and  $k = \frac{\omega}{c}$  is the wavenumber, '-' sign represents a forward wave, and the '+' sign represents a backward wave. The velocity of the particle oscillating back and forth is called particle velocity. It should be noted that this velocity is different from the rate of energy propagating through the medium, which is defined as the group velocity or the sound propagation speed. We shall characterize the acoustic wave by a pressure field p(x,t). In the case of a harmonic wave in a homogeneous medium, the particle displacement velocity in the acoustic field is given as:

$$v = \frac{(\nabla p)}{i\omega\rho} = \frac{A}{\rho c} \cdot e^{i(\omega t \pm kx)}$$
 (II.1.3)

where  $\rho$  is the density of the medium. The characteristic acoustic impedance is defined as:

$$Z = \frac{p}{v} = \frac{Ae^{i(\omega t \pm kx)}}{\frac{A}{\rho c} \cdot e^{i(\omega t \pm kx)}} = \rho c$$
 (II.1.4)

In general, the ultrasound imaging systems use pulsed ultrasound instead of continuous waves. It is assumed that the medium is non-dispersive (i. e. the speed of propagation c does not depend on the frequency of ultrasound). The time, t, for a pulse to travel a distance, d, through a non-dispersive medium is used to measure the speed, c, of ultrasonic propagation; where

$$c_{pulse} = \frac{2d}{t} \tag{II.1.5}$$

Thus if the speed in the medium is independent of frequency, the shape of the pulse (which may contain a wide range of frequency) remains unchanged as it propagates through the medium. If the pulse shape changes the pulse speed measurement in equation (II.1.5) is not precise since it relies upon some feature of the pulse shape (e.g. pulse peak). Few materials, however, are truly nondispersive, and pulse distortion to some extent is inevitable. Another source of pulse dispersion is due to propagating attenuation. It is well known that the higher frequencies suffer greater attenuation than lower frequencies, thus creating a situation where pulse distortion would be expected. A detailed discussion will occur in the next chapter.

The intensity of a wave is defined as the average power carried by the wave per unit area normal to the direction of propagation. For ultrasonic propagation, the intensity, i(t), is related to the medium velocity and pressure by the following relation:

$$i(t) = p(t) \cdot v(t) \tag{II.1.6}$$

For sinusoidal propagation, the average intensity, I, can be found by averaging i(t) over one cycle to obtain:

$$I = \frac{1}{2}p_0v_0 \tag{II.1.7}$$

where  $p_0$  and  $v_0$  represent peak values. However, most ultrasound imaging systems use pulsed waves and the intensity of the beam is not uniform. Therefore, there are two common intensity definitions used in the pulsed ultrasonic systems: spatial average-temporal average intensity (SATA) where the temporal average intensity is averaged over the beam cross section area in a specified plane (may be approximated as the ratio of ultrasonic power to the beam cross sectional area); and spatial peak-temporal average intensity (SPTA) where the value of the temporal average intensity is taken at a point in the acoustic field where temporal peak intensity is maximum.

#### II.2 Reflection and transmission of acoustic waves at a normal to the boundary

When a plane wave impinges normally on an interface between two different media (different characteristic acoustic impedance), it will be partially reflected and partially transmitted as shown in  $Figure \ \Pi.1$ . Let  $p_i$ ,  $p_r$  and  $p_t$  represent values of acoustic pressure for incident, reflected and transmitted waves, respectively, or

$$p_i \equiv p_i(x, t) = A_i e^{i(\omega t - k_1 x)}$$
 (II.2.1)

$$p_r \equiv p_r(x, t) = A_r e^{i(\omega t + k_1 x)}$$
 (II.2.2)

$$p_t \equiv p_t(x, t) = A_t e^{i(\omega t - k_1 x)}$$
 (II.2.3)

The symbols  $A_i$ ,  $A_r$  and  $A_t$  represent pressure amplitudes and  $k_1$  and  $k_2$  the wavenumber,  $\frac{2\pi}{\lambda}$ , for the two media. From equation (II.1.3), we can obtain the particle displacement velocities  $v_i$ ,  $v_r$  and  $v_t$  for the incident, reflected and transmitted waves, respectively, or

$$v_i = \frac{(\nabla p_i)}{i\omega \rho_1} = -\left(\frac{A_i}{\rho_1 c_1} \cdot e^{i(\omega t - k_1 x)}\right)$$
 (II.2.4)

$$v_r \equiv \frac{(\nabla p_r)}{i\omega \rho_1} = \frac{A_r}{\rho_1 c_1} \cdot e^{i(\omega t + k_1 x)}$$
(II.2.5)

$$v_t = \frac{(\nabla p_t)}{i\omega \rho_2} = -\left(\frac{A_i}{\rho_1 c_1} \cdot e^{i(\omega t - k_1 x)}\right)$$
 (II.2.6)

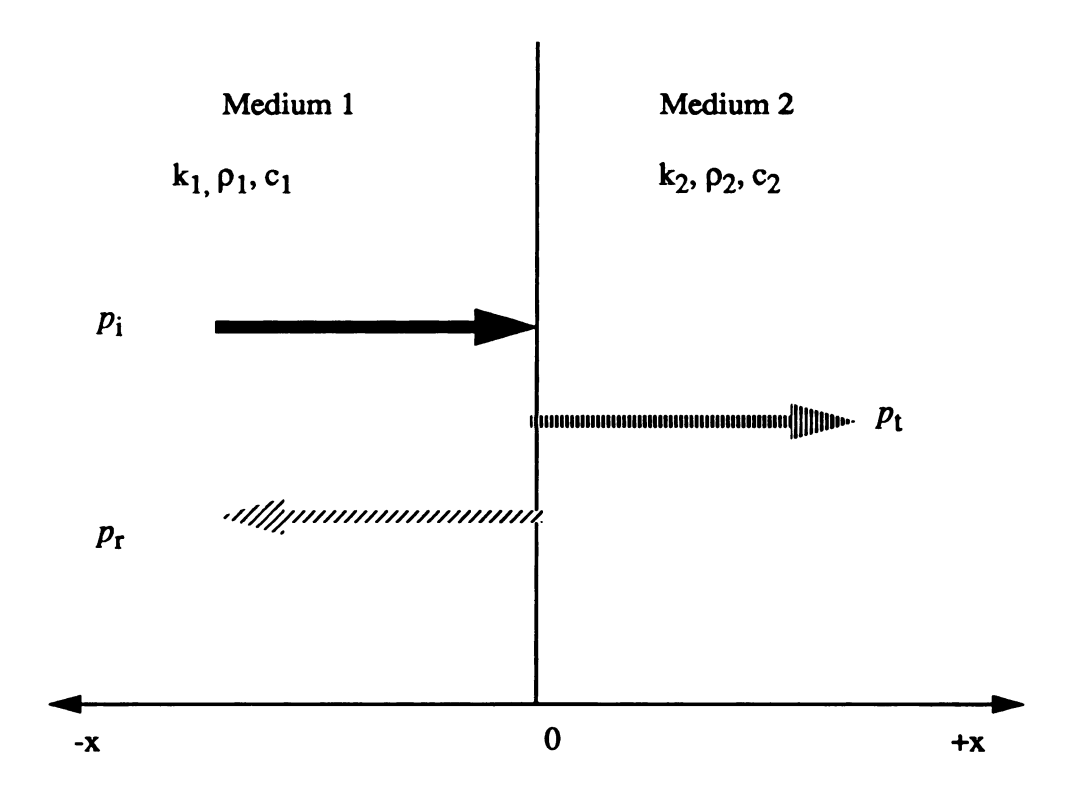


Figure II.1 Normal incident wave at interface between two different media with different acoustic impedance.

At the interface, the following conditions must be satisfied at all times:

(a) In order to preserve continuity, the pressure at the interface must be the same on both sides, or

$$p_{r}(0,t) = p_{r}(0,t) + p_{r}(0,t)$$
 (II.2.7)

(b) particle velocities normal to the interface must be equal on both sides, otherwise the two media would not remain in contact, so that:

$$v_{r}(0,t) = v_{r}(0,t) + v_{r}(0,t)$$
 (II.2.8)

From the above boundary conditions, one can define the pressure reflection coefficient,  $r = \frac{p_r(0, t)}{p_i(0, t)}$ , and the pressure transmission coefficient,  $t = \frac{p_t(0, t)}{p_i(0, t)}$ . Substituting equations (II.2.1)-(II.2.6) into equations (II.2.7) and (II.2.8), gives the pressure reflection coefficient and pressure transmission coefficient as follows:

$$r = \frac{p_r(0,t)}{p_i(0,t)} = \frac{\rho_2 c_2 - \rho_1 c_1}{\rho_2 c_2 + \rho_1 c_1} = \frac{Z_2 - Z_1}{Z_2 + Z_1}$$
 (II.2.9)

and

$$t = \frac{p_t(0,t)}{p_i(0,t)} = \frac{2(\rho_2 c_2)}{\rho_2 c_2 + \rho_1 c_1} = \frac{2Z_2}{Z_2 + Z_1} = 1 + r$$
 (II.2.10)

In order to derive the dual interrogation relationship, the reflection coefficient, r', and transmission coefficient, t', from the opposite direction incident waves, (i.e. the wave propagating from media 2 to media 1) must be obtained. These have the following relationships with respect to reflection coefficient, r, and transmission coefficient, t:

$$r' = -r \tag{II.2.11}$$

and

$$t' = 1 + r' = 1 - r \tag{II.2.12}$$

In general, the acoustic intensity, I, is proportional to the square of the amplitude of pressure,

$$I \propto |p(x,t)|^2 \tag{II.2.13}$$

It is possible to define an acoustic power reflection coefficient and a power transmission coefficient. At the interface, the ratio of the acoustic intensity of the reflected wave to that of the incident wave defines the acoustic power reflection coefficient, R, while the ratio of the intensity of the transmitted wave to that of the incident wave is the acoustic power transmission coefficient, T. Since the incident wave and the reflected wave propagates through the same medium, the acoustic power reflection coefficient is easily given by:

$$R = \frac{I_r}{I_i} = \frac{|p_r(0,t)|^2}{|p_i(0,t)|^2} = \left(\frac{Z_2 - Z_1}{Z_2 + Z_1}\right)^2$$
 (II.2.14)

While at the interface, the conservation of energy results in the acoustic power transmission coefficient:

$$T \equiv \frac{I_t}{I_i} = 1 - R = \frac{4Z_1Z_2}{(Z_2 + Z_1)^2}$$
 (II.2.15)

where  $I_i$ ,  $I_p$  and  $I_t$  are the intensity of the incident wave, reflected wave, and transmitted wave, respectively.

It is interesting to note the reciprocity that exits for the acoustic power reflection and transmission coefficient. For example, R and T have the same value whether the acoustic wave propagates from medium 1 to medium 2 or from medium 2 to medium 1, or:

$$R' = R \tag{II.2.16}$$

and

$$T' = 1 - R' = 1 - R = T$$
 (II.2.17)

where R' and T' represent the acoustic power reflection coefficient and the power transmission coefficient from the opposite direction of wave propagation. The behavior of both the pressure and the power at the boundary are important in ultrasound interrogation. Maximizing the power transfer is an important factor for designing efficient transducers. This can be accomplished through proper impedance matching of transducer and the receiving material. Moreover, the selection of using a coupling medium (i. e. a liquid or gel having an impedance similar to human tissue) between the transducer and tissue for diagnostic application is essential for generating a good power transfer.

#### II.3 Wave propagation with attenuation

Attenuation of acoustic energy during propagation is a complex phenomena. Two mechanism are primarily responsible for the attenuation, (1) the scatter of energy away from the acoustic pathway and, (2) absorption, in which the acoustic energy is transformed into another energy form. There is experimental evidence [55-56] to suggest that shear waves are so strongly damped that only compressional waves need to be considered in diagnostic medicine (0.5~20MHz) and material evaluation. Shear waves generated by mode conversion at inhomogeneities within the tissue will be so rapidly damped that their presence will not appear in pulse-echo measurements but their effect will be to contribute to the effective attenuation coefficient.

The absorption loss in liquids and solids, relaxation absorption [57], occurs as the wave propagates through material and neighboring particles intercept wavefronts moving

at different speeds. This attenuation loss can be quantified in the following way: For a plane acoustic pressure wave propagating through the material, the output acoustic pressure is:

$$p = p_0 exp(-\alpha(f)D)$$
 (II.3.1)

where

 $p_0$  = original pressure level at a reference point

p =pressure level at a second reference point

D = the traveled distance

and the frequency-dependent attenuation can be expressed as:

$$\alpha(f) = \alpha_0 f^n \tag{II.3.2}$$

where

 $\alpha_0$  = attenuation coefficient

n = exponent dependency

If the incident wave is a narrow-band signal, the attenuation,  $\alpha(f)$ , will not change appreciably with frequency over a range around the center frequency,  $f_c$ , where the incident energy is concentrated. The attenuation can be considered at the frequency  $f_c$ , and independent of frequency. Under this assumption, we can describe the wave propagating through a multi-layered structure; the amplitude reduced by attenuation, reflection coefficient and distance traveled as shown in *Figure II.2*. This model will be employed for the time domain analysis.

A narrow-band signal is very difficult to realize in conventional ultrasonic systems. Therefore, the attenuation,  $\alpha$ , independent of frequency will not hold. In general, the

magnitude of the transfer function,  $H_i(f)$ , can be characterized by:

$$|H_i(f)| = exp(-\alpha_i(f)D_i)$$
 (i=1,....,N) (II.3.3)

where  $\alpha_i(f) = \beta_i f^n$ , and  $\beta_i$  is the attenuation coefficient of the *i-th* layer medium. The wave propagating through multi-layered structures can be described in the frequency domain. Specifically, the spectrum can be given by the transform of the incident signal convolved with the attenuation process and associated reflection coefficients, so that:

$$Y_i(f) = r_i \prod_{k=1}^{i-1} (1 - r_k^2) |H_i(f)|^2 |X(f)|$$
 (i=1,...,N) (II.3.4)

This frequency domain model is shown in Figure II.3.

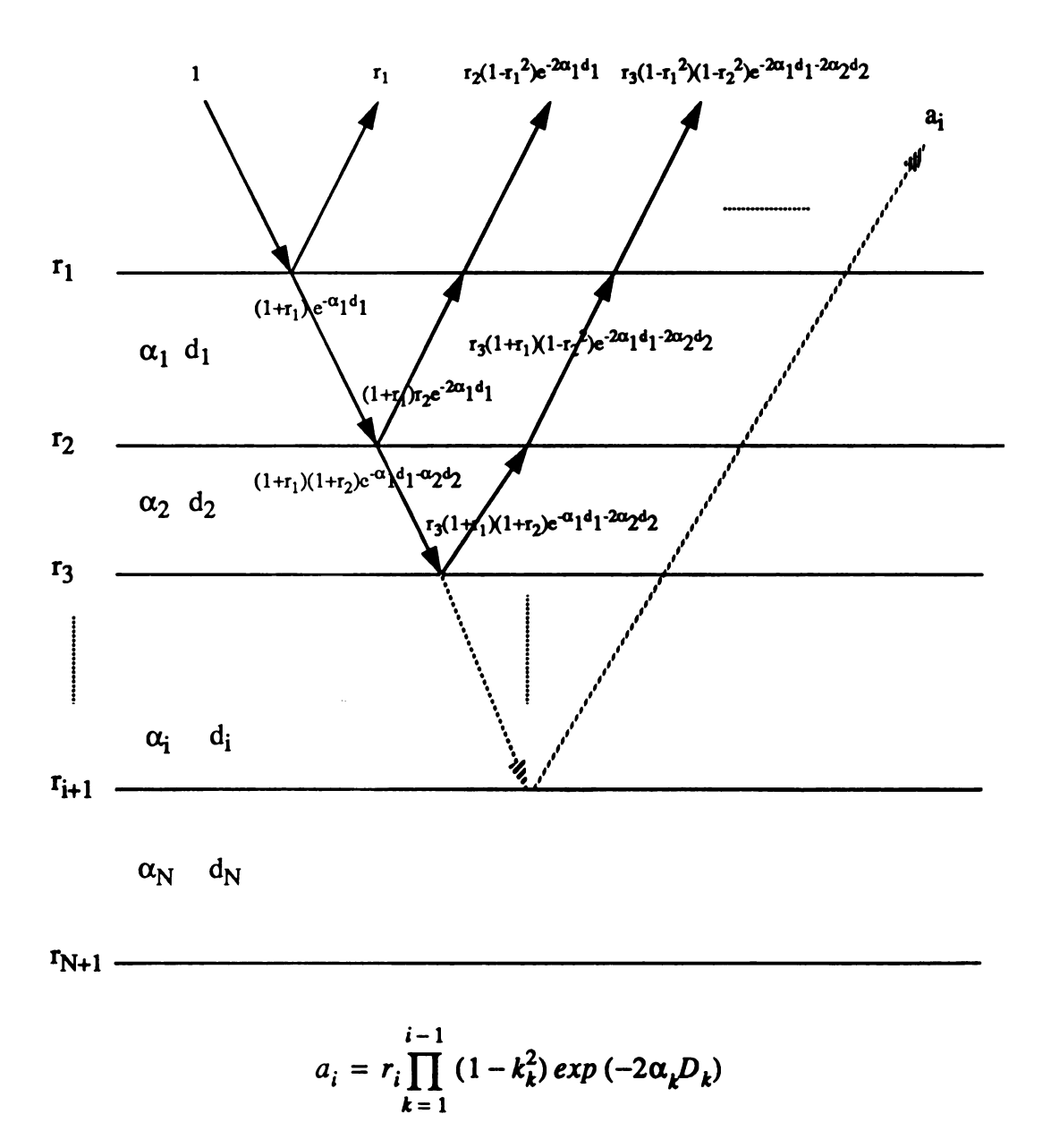
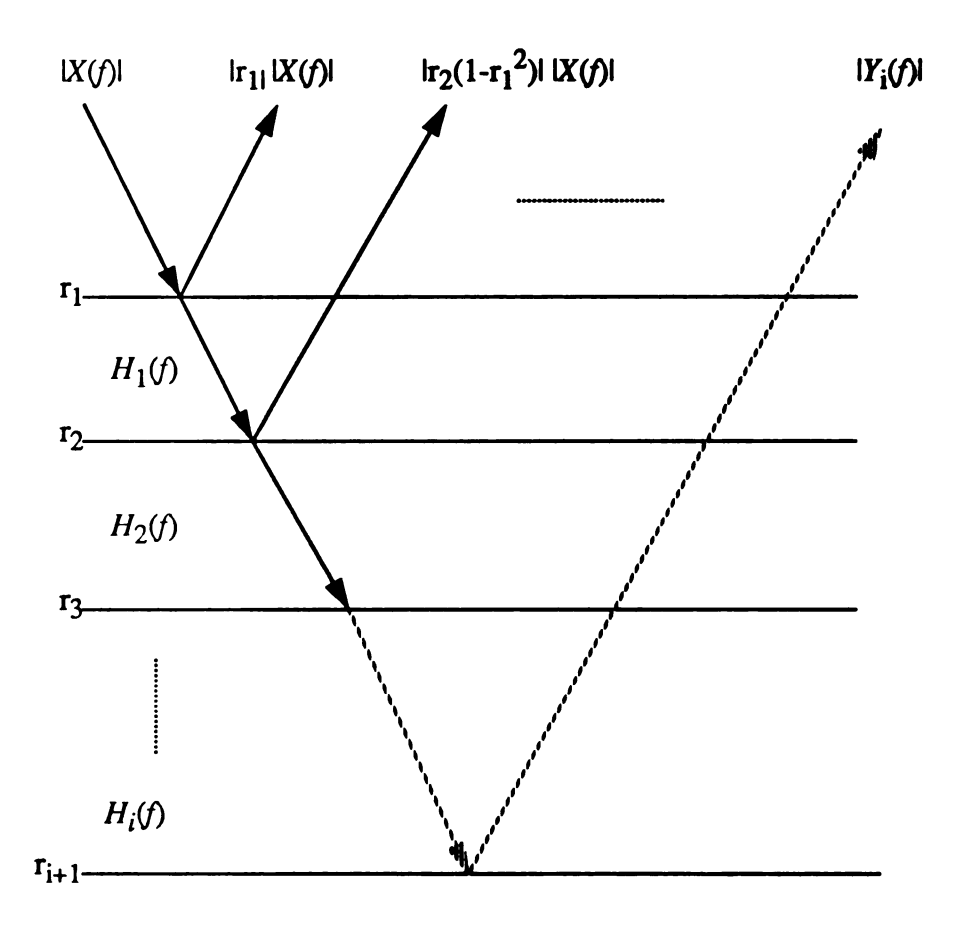


Figure II.2 The ultrasonic wave propagating through multi-layered material affected by reflection coefficient and attenuation under a narrow-band incident signal assumption.



$$Y_i(f) = r_i \prod_{k=1}^{i-1} (1 - r_k^2) |H_i(f)|^2 |X(f)|$$

Figure II.3 The wave propagating through a multi-layered structure described in the frequency domain.

# **CHAPTER III**

# TIME DOMAIN ANALYSIS FOR MULTI-LAYERED MATERIAL

#### III.1 Limitations and advantages of time domain techniques

The time domain technique extracts information on material properties, attenuation coefficient, acoustic impedances and propagation velocity, from a purely one-dimensional echo sequence (A-mode signals). The major limitations of this technique are: (I) The difficulty of resolving consecutive echoes from the layered object when the thickness of the sample is small compared with the pulse width (i. e. echo overlapping), and (II) the difficulty of accounting for frequency dependent attenuation. To resolve echo overlap, deconvolution is used to enhance the resolution [24-29], however, this increases the computational complexity. The received signals deconvolved with the incident signal generate the impulse response of the target. This can resolve two boundaries by separating locations of peaks of the impulse response. For the cases where frequency dependent attenuation is not linear or quadratic, a closed form solution for the impulse response is not possible. Thus, it becomes impossible to obtain the attenuation coefficient from the impulse

response. The frequency attenuation dependence present in the incident pulse propagating through the medium, with frequency components attenuated by different degrees, results in pulse shape distortion. The reduction in pulse amplitude with distance will not follow the commonly assumed exponential law,  $\exp(-\alpha f_c^n D)$ , where  $\alpha$  is the attenuation coefficient,  $f_c$  is the center frequency of the incident pulse and D is the distance traveled. The deviation from exponential form is a function of pulse width, attenuation coefficient and the distance traveled (see section III.3). In spite of these limitations, time domain processing provides an excellent possibility for real time imaging because of its short processing time.

J. P. Jones [30] derived the acoustic impedance profiles of multi-layered material from the integral of the impulse response of a test target under the assumption of equal reflection coefficients at each boundary and non-attenuating medium. These two assumptions are rather restrictive and not practical for modeling a multi-layered structure. The accuracy of the impulse response is strongly dependent on the form of the incident signal as well as the particular deconvolution algorithm utilized. Since the acoustic impedances are related by the integral of the impulse response, the errors associated with its integral are larger than the impulse response itself. The relationships between the acoustic impedance and integral of the impulse response are obtained under the assumption of non-attenuating media. However, the attenuation process is actually the dominant factor for the interrogating wave, unless the layer thicknesses are very small, so that the erroneous results from this technique are predictable.

P. Cobo-Parra et al. [31] estimated the impedance profiles and overall attenuation of layered ocean floors by impulse response decovolution and an inversion algorithm. First, he estimated the overall attenuation coefficient of the whole sedimentary column from the logarithmic regression on the spectral ratios of nonoverlapped replicas (this step is similar

to the spectral difference method.). Secondly, he separated the attenuation factors from the impulse response and generated the impedance profiles. His treatment of the attenuation is simplified by the hypothesis of frequency linearity, and that the acoustic thickness for each layer should be equal. It is not always practical to model a multi-layered medium with the same acoustic thickness for each layer. The computations are complicated and the accuracy depends on the signal-to-noise ratio which is not easily obtained experimentally. In spite of the simplified model—the individual attenuation coefficients for each layer, cannot be determined.

A narrow-band pulse echo amplitude attenuation estimation method was described by Ophir et al. [58]. The technique assumes that the excitation is essentially monochromatic, with a single frequency continuous wave approximated by a finite duration pulse. The approach utilizes the difference in the log of the mean amplitudes from two planes divided by the plane separation to estimate the attenuation coefficient over some band of frequencies. They eliminated the beam profile variation effects by axial translation of the transducer such that the plane of interest remains at a constant range. This method must neglect the reflection coefficient between the boundaries which is a dominant factor in pulse echo amplitude reduction Thus the Ophir approach can not be employed for multi-layered material properties measurements.

Kak et al. [46] derived the attenuation coefficient for linear frequency-dependent media equal to  $2\pi$  times the root-mean-square duration of the impulse response of the layer. Measurement of attenuation therefore reduces to estimating the time between the impulse response from the incident and from the received waveforms. Although the deconvolution scheme can be performed either in the time domain or in the frequency domain, it will involve complicated computations. Moreover, the formulation assumes that the reflection coefficients (or transmittances) can be neglected so that the technique can not be employed

for multi-layered material.

#### III.2 Evaluation of multi-layered material properties by time domain techniques

Consider a multi-layered structure, as shown in *Figure III.*1, where  $\alpha_i$ ,  $Z_i$ ,  $r_i$  and  $D_i$  are the attenuation coefficients, acoustic impedances, reflection coefficients and layer thickness, respectively. In order to simplify the analysis, the following assumptions are made:

- (1.) The object under investigation consists of parallel homogeneous layers with the incident signal normal to the boundaries.
- (2.) Wave propagation through the medium is a linear time-invariant process.
- (3.) A narrow band transducer is used so that the attenuation process can be modeled as  $\exp(-\alpha x)$ , where  $\alpha$  is the attenuation coefficient at the center frequency,  $f_c$ , of the incident wave, x is the distance traveled.
- (4.) Higher order multiple reflections can be ignored, or eliminated by suitable gating.
- (5.) The thickness of layers are large compared to the incident pulse width(i.e. the return echoes do not overlap).

By using the convolution theorem, the relationship between the received echo signal, Y(t), and the incident signal, x(t), can be expressed as:

$$Y_1(t) = \int_{-\infty}^{\infty} x(\tau) h_1(t-\tau) d\tau$$
 (III.2.1)

and

$$Y_2(t) = \int_{-\infty}^{\infty} x(\tau) h_2(t-\tau) d\tau$$
 (III.2.2)

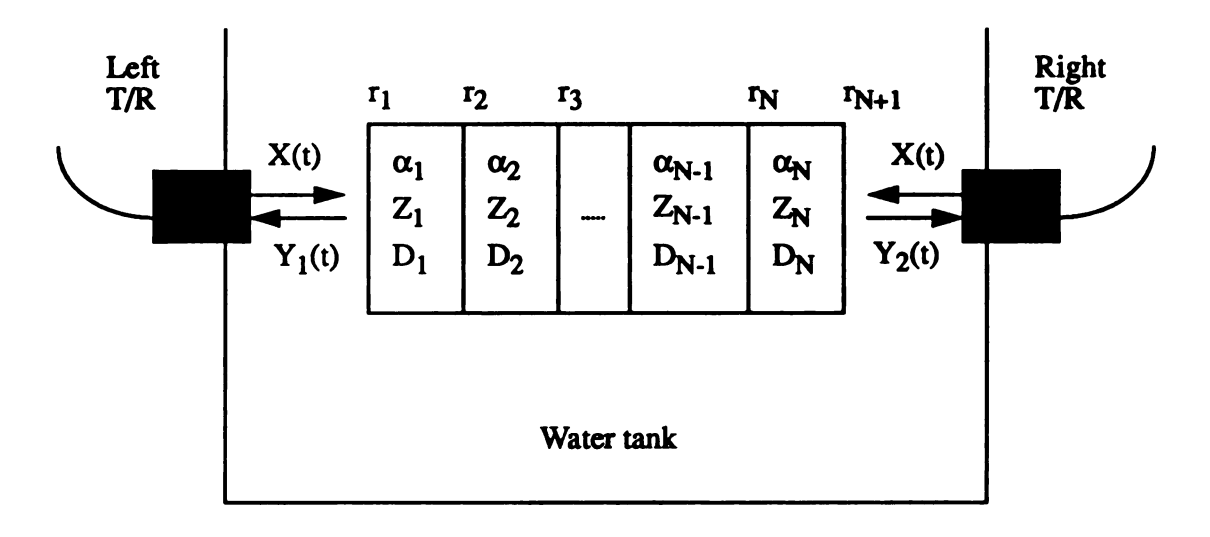


Figure III.1. Dual pulse-echo interrogation of a layered structure.

where  $Y_1(t)$  and  $Y_2(t)$  are the received echo signals from the left-side and right-side respectively, while  $h_1(t)$  and  $h_2(t)$  are the left-side and right-side impulse response of the test object. In general, the estimation of  $h_1(t)$  and  $h_2(t)$  from the measurement  $Y_1(t)$  and  $Y_2(t)$  is called deconvolution, or system identification. There are many deconvolution processes for improving resolution [24-29], but only a few for obtaining the attenuation properties, because they lack mathematical rigor except for linear or quadratic frequency-dependent attenuation [46]. The impulse responses of targets are not ideal delta functions [46]. J. P. Jones [30] expressed the impulse response by a sequence of delta functions under the assumption of waves propagating through non-attenuating media. Under the assumption (3) above, we can express the received echo signals,  $Y_i(t)$  i=1 or 2, as a sequence of delayed incident signals (i.e. amplitude reduction in terms of reflection coefficients and frequency-independent attenuation), or the impulse response of the target is:

$$h_1(t) = \sum_{i=1}^{N} a_i \delta(t - t_i)$$
 (III.2.3)

where  $a_i$  is the echo peak amplitude at  $t=t_i$ . The values of  $a_i$  can be related to the attenuation coefficient  $\alpha_i$ , layer thickness  $D_i$  and reflection coefficients  $r_i$  (for the boundary between the (i-1) th and i th layer) by:

$$a_i = exp(-2\alpha_0 D_0) r_i \prod_{k=1}^{i-1} (1 - r_k^2) exp(-2\alpha_k D_k)$$
 (i=1,....,N)

Similarly, the impulse response from the right side is:

$$h_2(t) = \sum_{j=1}^{N} b_j \delta(t - t_j)$$
 (III.2.5)

where  $b_j$  corresponds to the amplitude of the echo reflected from the boundary between the (j-1) th and j th layer. The amplitude  $b_j$  has the following form:

$$b_{j} = -exp(-2\alpha_{j}D_{j})r_{j}\prod_{k=j+1}^{N}(1-r_{k}^{2})exp(-2\alpha_{k}D_{k}) \quad (i=1,...,N) \quad (III.2.6)$$

The minus sign accounts for the fact that the reflection coefficient changes sign when the incident wave is from the opposite side of the object. The magnitude  $a_i$  and  $b_j$  (i, j=1, 2, ..., N) can be read directly from the impulse responses  $h_1(t)$  and  $h_2(t)$  from the dual pulse echo measurements shown in Figure III.2.

The amplitude ratio of successive echoes can be expressed as:

$$\frac{a_i}{a_{i+1}} = \frac{r_i}{r_{i+1}(1-r_i^2)\exp(-2\alpha_i D_i)}$$
 (i=1,...,N) (III.2.7)

and

$$\frac{b_i}{b_{i+1}} = \frac{r_i (1 - r_{i+1}^2) \exp(-2\alpha_i D_i)}{r_{i+1}}$$
 (i=1,...,N) (III.2.8)

The product of equations (III.2.7) and (III.2.8) gives:

$$\frac{a_i b_i}{a_{i+1} b_{i+1}} = \frac{r_i^2 (1 - r_{i+1}^2)}{(1 - r_i^2) r_{i+1}^2}$$
 (i=1,....,N) (III.2.9)

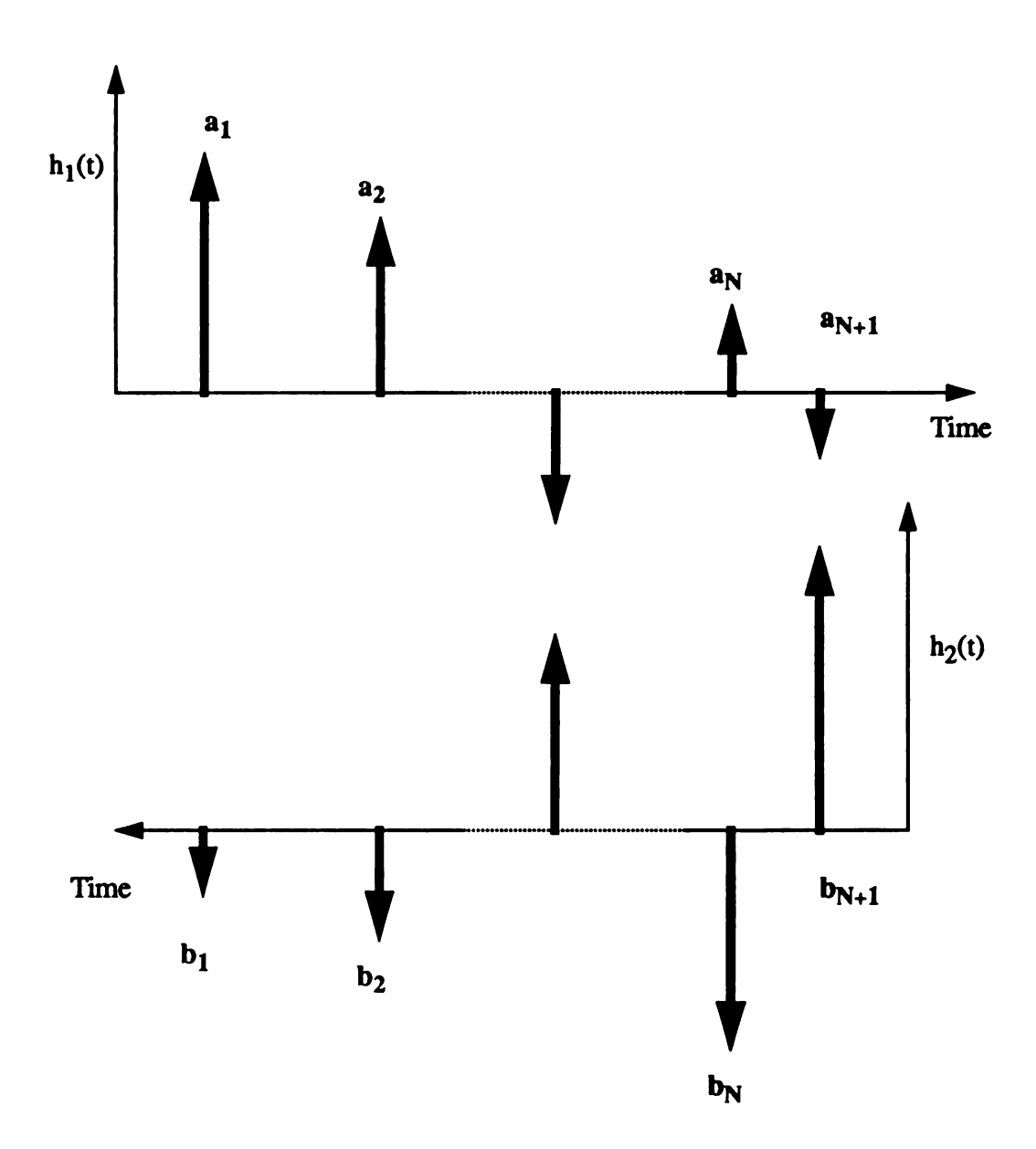


Figure III.2 Impulse responses of the dual interrogation configuration.

If we define a new parameter  $R_i$  as:

$$R_i = \frac{r_i^2}{1 - r_i^2}$$
 (i=1,....,N) (III.2.10)

then equation (III.2.9) can be reduced to:

$$\frac{a_i b_i}{a_{i+1} b_{i+1}} = \frac{R_i}{R_{i+1}}$$
 (i=1,....,N) (III.2.11)

The R parameters for successive layers are related by:

$$R_{i+1} = R_i \left[ \frac{a_{i+1}b_{i+1}}{a_ib_i} \right]$$
 (i=1,....,N) (III.2.12)

The reflection coefficient  $r_i$ , at an impedance discontinuity, can be expressed in terms of  $R_i$ , as follows:

$$r_i = S_i \sqrt{\frac{R_i}{1 + R_i}}$$
 (ii=1,....,N+1) (III.2.13)

where

$$S_i = \begin{pmatrix} 1 & (a_i > 0) \\ -1 & (a_i < 0) \end{pmatrix}$$

From the amplitude ratios, equations (III.2.7) and (III.2.8) give:

$$\frac{a_i b_{i+1}}{a_{i+1} b_i} = \frac{1}{(1-r_i^2) (1-r_{i+1}^2) \exp(-4\alpha_i D_i)}$$
 (i=1,....,N) (III.2.14)

Therefore the attenuation coefficient,  $\alpha_i$ , of the i th layer, is:

$$\alpha_i = \frac{1}{4D_i} ln \left[ \frac{a_i b_{i+1}}{a_{i+1} b_i} (1 - r_i^2) (1 - r_{i+1}^2) \right]$$
 (i=1,....,N) (III.2.15)

Observing above equation (III.2.15), we can find that, once the reflection coefficients are determined and the layer thicknesses are available, the attenuation coefficients for each layer can be obtained. The following algorithm can be used to find the reflection coefficient at each boundary and the attenuation coefficient in each layer:

1. The reflection coefficient of the first interface is evaluated from the following:

$$r_1 = a_1 exp(2\alpha_0 D_0)$$
 (III.2.16)

where  $a_1$  is obtained from the impulse response function. The transducers are immersed in a coupling medium (usually water), so that the attenuation coefficient  $\alpha_0$  is assumed known. The distance between transducer and test object  $D_0$  is a fixed distance which can be measured. In practice, it is rather difficult to get a replica of the incident pulse from the transmitter/receiver transducer. Therefore, the simple experimental setup in Figure III.3 is suggested to obtain the reflection coefficient  $r_1$  at the first boundary (detailed description see next paragraph)

2. The reflection coefficient,  $r_{i+1}$ , of successive interfaces can be obtained once the parameter  $R_i$  is found, by:

$$R_{i+1} = R_i \left[ \frac{a_{i+1}b_{i+1}}{a_ib_i} \right]$$
 (i=1,....,N)

and

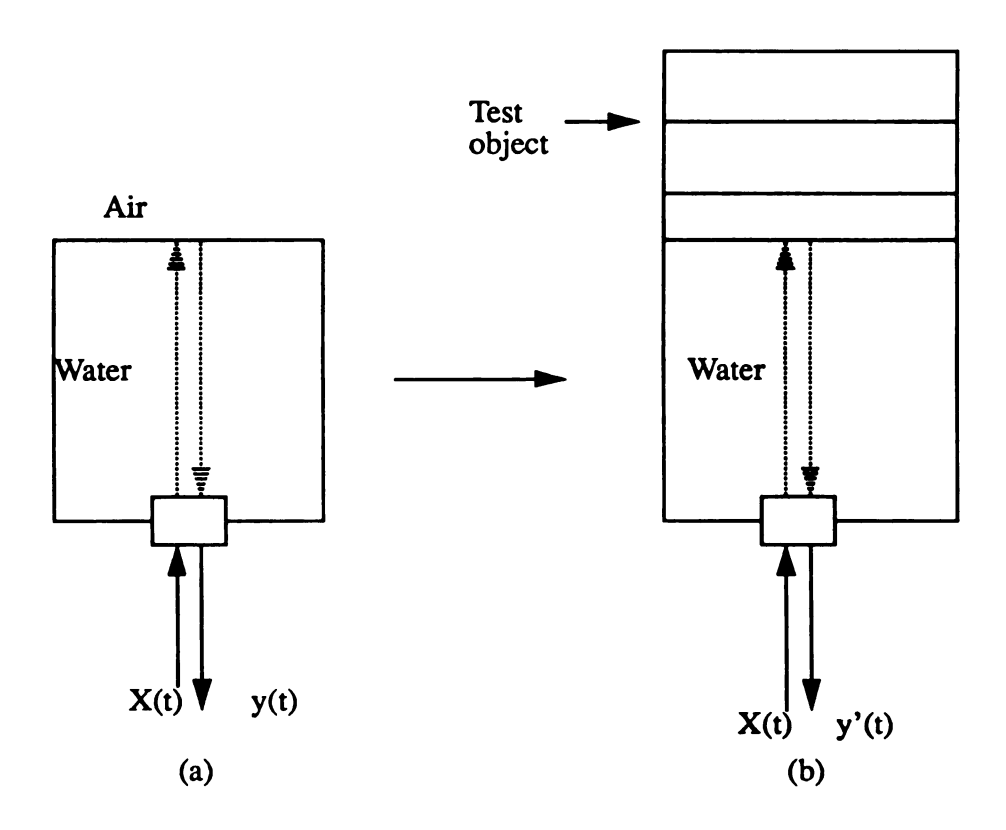


Figure III.3 Experimental setup for measuring  $r_1$ , (a) configuration for reference (b) comparing the amplitude y'(t) with y(t) to obtain  $r_1$ .

$$r_i = S_i \sqrt{\frac{R_i}{1 + R_i}}$$
 (III.2.18)

where

$$S_i = \begin{pmatrix} 1 & (a_i > 0) \\ -1 & (a_i < 0) \end{pmatrix}$$

Therefore, the acoustic impedances for each layer can be related by:

$$Z_i = \frac{1+r_i}{1-r_i} \cdot Z_{i-1}$$
 (i=1,....,N)

Once the acoustic impedance of water,  $Z_0$ , is known, the acoustic impedance for each layer can be iteratively obtained.

3. From the  $r_i$ ,  $R_i$ , amplitudes  $a_i$  and  $b_i$ , and known  $D_i$ , the attenuation coefficients  $\alpha_i$  can be explicitly evaluated from equation (III.2.15). D cannot be measured directly from the A-mode echo sequence - it is a distance which is inferred from the measurement of time delay between two echoes. A precise specification of D would require knowledge of the mean sound velocity in each material layer. Therefore, we can only obtain the attenuation-velocity product  $(\alpha v)$  from the experimental data [59].

The procedure of obtaining the first reflection coefficient,  $r_1$ , is described as follows: The impedance of air is assumed negligible compared to that of water (i. e.  $Z_{air} \ll Z_{water}$ ) and the reflection coefficient at water / air interface equals approximately -1. Therefore, the amplitudes of y(t) and y'(t), in *Figure III.3*, can be expressed as:

$$y_{peak}(t) = -A_0 e^{-2\alpha_0 D_0}$$
 (III.2.20)

and

$$y_{peak}'(t) = r_1 A_0 e^{-2\alpha_0 D_0}$$
 (III.2.21)

where

 $A_0$  = the amplitude of the incident pulse

 $\alpha_0$  = attenuation coefficient of water

 $D_0$  = the distance of the coupling media

 $r_1$  = the reflection coefficient at the first boundary of the target

From equations (III.2.20) and (III.2.21), the reflection coefficient  $r_1$  is given by:

$$r_1 = -\frac{y_{peak}(t)}{y_{peak}(t)}$$
 (III.2.22)

Therefore, we do not require information from the incident pulse at the in transmitter / receiver to obtain  $r_1$ .

# 3.3 Accuracy of time domain technique for attenuation measurement

Although the time domain technique proposed in the previous section provides a simple way to evaluate the multi-layered material properties, it was developed under a narrow-band incident signal assumption. Actually, in order to obtain narrow-band signals, the ultrasonic pulse duration must increase, which reduces axial resolution. The spectrum

of the incident wave in our experimental setup is shown in *Figure* III.4, Clearly, this is not a truly narrow-band signal, since the bandwidth of the incident signal is about 1.8 MHz. Because the incident acoustic wave is not truly narrow-band, an erroneous result will occur when utilizing the peak amplitude in the time domain. The error incurred by using time domain techniques to evaluate the attenuation of material, which is frequency dependent, is discussed next. In order to gain insight into how the bandwidth affects the signal measurements, we will assume Gaussian incident pulses.

In order to obtain a Gaussian shaped spectral signal, we assume the incident pulse has the Gaussian-shape:

$$x(t) = e^{-\frac{t^2}{2\sigma^2}} \cdot e^{j2\pi f_0 t}$$
 (III.3.1)

where  $f_0$  is the center frequency, t is time and  $\sigma$  is the standard deviation. The signal and its spectrum are related by the Fourier transform pair [60]:

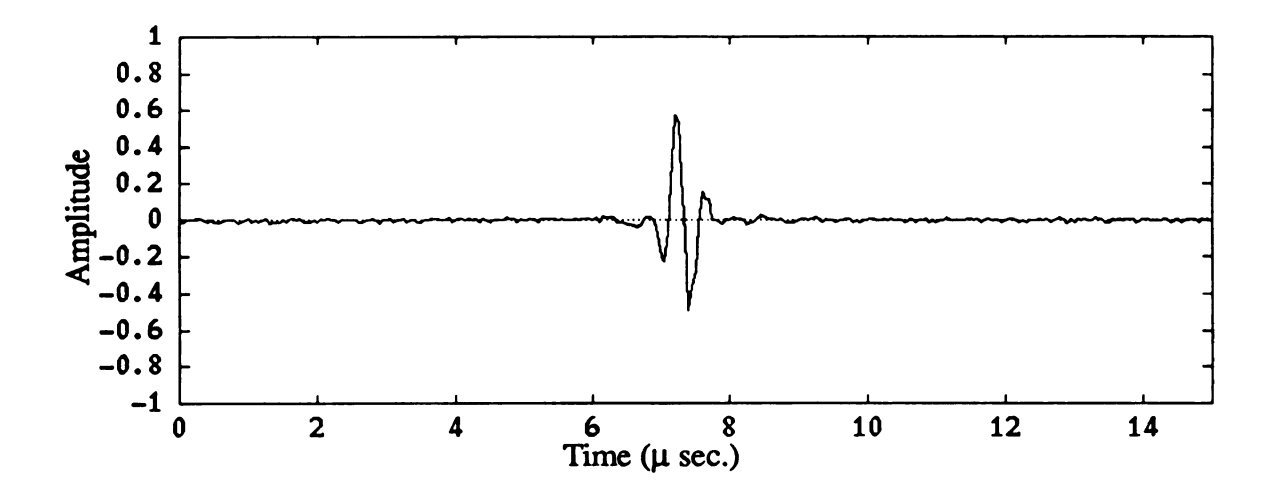
$$X(f) = \int_{-\infty}^{\infty} x(t) e^{-j2\pi f t} dt$$

$$x(t) = \int_{-\infty}^{\infty} X(f) e^{j2\pi f t} df$$
(III.3.2)

The spectrum of the incident pulse can thus be obtained by:

$$X(f) = \int_{-\infty}^{\infty} x(t) e^{-j2\pi f t} dt = \sqrt{2\pi} \sigma e^{-2\pi^2 \sigma^2 (f - f_0)^2}$$

$$= \sqrt{2\pi} \sigma exp \left( -\frac{(f - f_0)^2}{2\sigma_f^2} \right)$$
 (III.3.3)



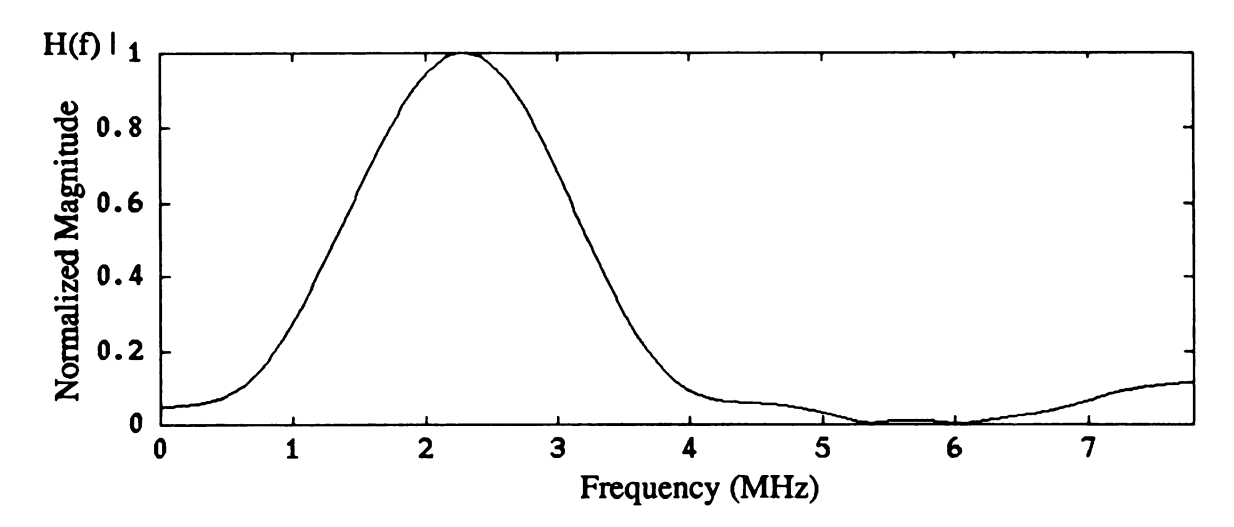


Figure III.4 Time and frequency domain representation of the incident signal.

where  $\sigma_f^2 = 1/(4\pi^2\sigma^2)$  is the variance of the incident spectrum, equal to 0.18 B<sup>2</sup>, B is the half amplitude bandwidth.

The transfer function of the medium can be characterized by:

$$H(f) = exp(-\alpha f^{n}D) \cdot e^{-jkD}$$
 (III.3.4)

where  $\alpha$  is the attenuation coefficient, D is the distance traveled, n is equal to 1 or 2, and  $k=2\pi f/v$  is the wave number with phase velocity, v, assumed constant for a nondispersive medium, and the output y(t) for a linear time invariant system is:

$$y(t) = x(t) \cdot h(t)$$

and

$$Y(f) = X(f)H(f)$$
(III.3.5)

Two attenuation cases can now be considered:

**CASE I** n=1 
$$H(f) = e^{-\alpha Df} \cdot e^{-j2\pi f \frac{D}{v}}$$

The output spectrum for this case is given by:

$$Y(f) = X(f)H(f) = \sqrt{2\pi}\sigma e^{-2\pi^2\sigma^2(f-f_0)^2} \cdot e^{-\alpha Df} \cdot e^{-j2\pi f\frac{D}{\nu}}$$
 (III.3.6)

and

$$y(t) = \int_{-\infty}^{\infty} Y(f) e^{j2\pi ft} df$$

$$= \int_{-\infty}^{\infty} \left[ \sqrt{2\pi} \sigma e^{-2\pi^2 \sigma^2 (f - f_0)^2} \cdot e^{-\alpha Df} \cdot e^{-j2\pi f \frac{D}{\nu}} \right] e^{j2\pi f t} df$$

$$= exp\left(-\alpha Df_0 + \frac{\alpha^2 D^2}{8\pi^2 \sigma^2}\right) \cdot exp\left\{-\frac{\left(t - \frac{D}{v}\right)^2}{2\sigma^2}\right\}$$

$$\cdot exp\left\{j2\pi\left(\left(f_0 - \frac{\alpha D}{4\pi^2 \sigma^2}\right)\right)\left(t - \frac{D}{v}\right)\right\} \qquad (III.3.7)$$

Observing equation (III.3.7), when t=D/v, one can obtain the peak amplitude, y(D/v), in the time domain signal:

$$y_{peak}(t) = y(\frac{D}{v}) = exp\left(-\alpha Df_0 + \frac{\alpha^2 D^2}{8\pi^2 \sigma^2}\right)$$
 (III.3.8)

Hence, it is apparent that the decay of the peak amplitude in the time domain will not follow strictly the exponential  $\exp(-\alpha D f_0)$ . From equation (III.3.8), if  $\alpha D$  is very small (low attenuation) or  $\sigma^2$  is very large (narrow-band signal approximation),  $\frac{\alpha^2 D^2}{8\pi^2 \sigma^2}$  approaches zero. For this case we can accurately measure the attenuation in the time domain by following the signal peak amplitudes.

CASE II n=2. 
$$H(f) = exp(-\alpha f^2 D) \cdot e^{-i2\pi f \frac{D}{v}}$$

The output spectrum for this case is given by:

$$Y(f) = X(f) \cdot H(f)$$

$$= \sqrt{2\pi}\sigma \cdot exp\left\{-\left(\alpha D + 2\pi^2\sigma^2\right)\left(f - \frac{2\pi^2\sigma^2f_0}{2\pi^2\sigma^2 + \alpha D}\right)^2\right\}$$

$$\cdot exp \left\{ -(2\pi^2 \sigma^2 f_0) \left( 1 - \frac{2\pi^2 \sigma^2 f_0}{2\pi^2 \sigma^2 + \alpha D} \right) \right\} \cdot exp \left( -j2\pi f \frac{D}{\nu} \right)$$
 (III.3.9)

After the inverse Fourier transformation operation, one can obtain the output signal in the time domain:

$$y(t) = \int_{-\infty}^{\infty} Y(f) e^{j2\pi ft} df$$

$$= \sqrt{\frac{1}{1 + \frac{\alpha D}{2\pi^2 \sigma^2}}} \cdot exp\left(-\frac{\alpha Df_0^2}{1 + \frac{\alpha D}{2\pi^2 \sigma^2}}\right) \cdot exp\left\{-\frac{\left(t - \frac{D}{v}\right)^2}{2\sigma^2 \left(1 + \frac{\alpha D}{2\pi^2 \sigma^2}\right)}\right\}$$

$$\cdot exp\left\{j2\pi\left(\frac{f_0}{1+\frac{\alpha D}{2\pi^2\sigma^2}}\right)(t-\frac{D}{\nu})\right\}$$
 (III.3.10)

When t=D/v, we obtain the peak amplitude in the time domain for the output signal, y(D/v):

$$y_{peak}(t) = y(\frac{D}{v}) = \sqrt{\frac{1}{1 + \frac{\alpha D}{2\pi^2 \sigma^2}}} \cdot exp\left(-\frac{\alpha D f_0^2}{1 + \frac{\alpha D}{2\pi^2 \sigma^2}}\right) \quad \text{(III.3.11)}$$

Again, it is apparent that the decay of the peak amplitude in the time domain signal will not follow a simple exponential law  $exp(-\alpha Df_0^2)$ . If  $\alpha D$  is very small (low attenuation) or  $\sigma^2$  is large (narrow-band approximation) so that,  $\frac{\alpha D}{2\pi^2\sigma^2} \rightarrow 0$ , we can accurately measure the attenuation in the time domain by following the signal peaks.

From the above derivation, we can find the attenuation of material subject to the appropriate assumptions. However, the only factor which can be controlled is the bandwidth of the incident signal. The larger the bandwidth used, the larger the resultant error in the measurements. The theoretical peak amplitude error,  $exp\left(\frac{\alpha^2D^2}{8\pi^2\sigma^2}\right)$ , for a wave propagating through 2.0 cm and 1.0 cm plexiglass is shown in *Figure III.5*. Although a small bandwidth of the incident signal will give a good attenuation estimate, it will give very poor range resolution.

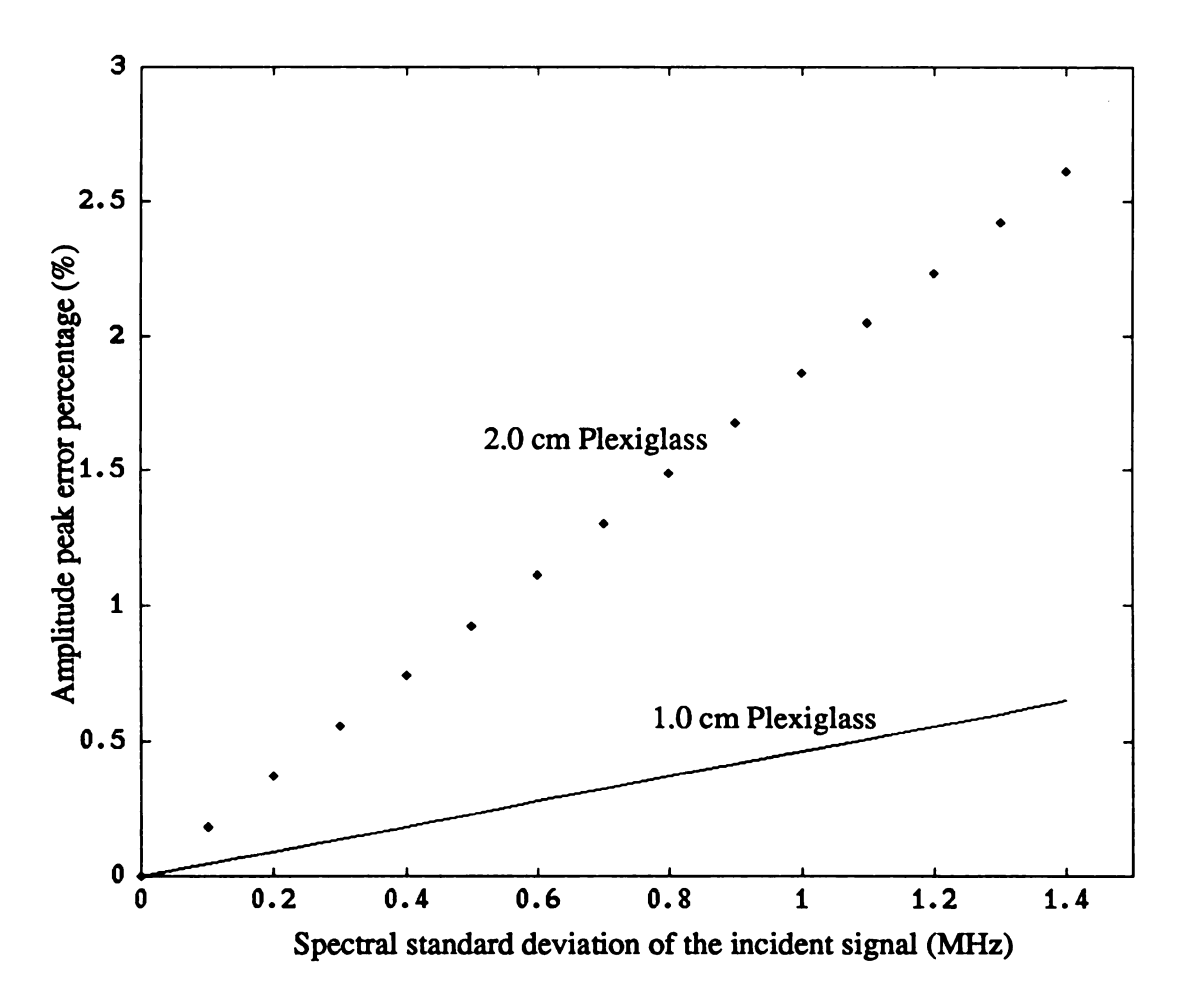


Figure III.5 The theoretical peak amplitude error of the interrogating wave passing through 2.0 cm and 1.0 cm plexiglass.

# **CHAPTER IV**

# FREQUENCY DOMAIN ANALYSIS FOR MULTI-LAYERED MATERIAL

#### IV.1 Comparison of the spectral difference and spectral shift methods

The frequency domain approaches which utilize broadband signals for estimating the attenuation can be broadly divided into the spectral difference and the spectral shift methods. The spectral difference method [7,10,61,62] estimates the attenuation,  $\alpha(f)=\alpha_0 f^n$ , by fitting the spectral difference between the input and output signals. Therefore, no specific spectral form of the incident pulse is required to estimate the parameters  $\alpha_0$  and n, where n is not restricted to be an integer. Kuc [9] estimates  $\alpha_0$  for liver by comparing the spectrum of a broadband pulse reflected from a planar interface, with and without a volume of liver interposed, under the assumption of linear-dependent attenuation and ignorance of the reflection coefficient between the coupling media (usually water) and the liver. This assumption is reasonable in this case since the impedance of the coupling medium is similar to that of tissue so that the reflection coefficient at this boundary can be neglected. Insana et al. [52] modified the spectral difference method to improve the overall measurement

accuracy. The Insana modification involved counting for the transducer beam diffraction pattern in the data analysis by using empirically determined correction factors. In general, the spectral difference between the input and output signals contains information on both the attenuation and reflection coefficient. These material properties can not be determined simply by using the signal information in a single trace of the echo return. Some authors [10-11] ignore the effect of the reflection coefficient or assume it a known quantity [2,46]. In reality, the reflection factor does exist at an interface between two different acoustic impedance media, and it is an important factor governing the reduction in spectral power of the reflected signals. The absence of a reflection coefficient is acceptable in transmission techniques (where the broadband pulse passes through the tissue of interest and is received by a second transducer.) for measuring the tissue attenuation, of material with acoustic close to that of water. The measurement is carried out using a substitution method in which the received signal obtained with only water between the transducers is compared with the received signal obtained when the tissue is substituted. Although the transmission technique is usually not suitable for clinical use, it provides a valuable reference point for evaluating approaches based on reflected ultrasound. When a multi-layered structure is considered, the transmission technique provides the accumulated attenuation, rather than the individual attenuation for each layer. Therefore, the reflected pulse interrogation should be employed and the reflection coefficient be considered for multi-layered material investigation.

When an ultrasound pulse passes through an attenuating medium, it experiences a frequency-dependent attenuation. The attenuation experienced at higher frequencies is larger than at lower frequencies. This results in a down-shift of the center frequency of the spectrum after passage through a lossy medium. The spectral shift technique for ultrasound propagation through frequency-dependent media was originally suggested by Serabian [47]. He experimentally showed the downshift in center frequency for a pulse propagating

through different thicknesses of graphite material which has very high attenuation. Kuc [7-10] applied this concept to evaluate attenuation in linear frequency-dependent soft tissue. Dines and Kak [2] employed the transmission substitution technique and spectral-shift method to estimate the overall attenuation of multi-layered tissue which models the lineardependent attenuation with different attenuation coefficients for each layer. J. Ophir et al. [51] extended the method to nonlinear frequency-dependent media. The spectral shift approach requires a Gaussian-shaped spectrum for the interrogating pulse. However, it does not require knowledge of the reflection coefficient or transmittance for estimating the attenuation. Most imaging systems place no constraint on the transmitted signal other than that it be of short duration. By slightly modifying the transducer driving voltage and impedance loading, a Gaussian-shaped pulse with a corresponding Gaussian power spectrum can be produced. The effect of the linear attenuation on a Gaussian spectrum is readily shown to shift the peak to lower frequencies while maintaining the same Gaussian shape. For the nonlinear frequency-dependent attenuation medium, the Gaussian shape remains but the shape becomes narrower (i. e. the standard deviation is less than that of the incident pulse spectrum). Narayana et al. [49] derived the theoretical relation between the center frequency downshift and the spectral bandwidth with a sinc(x) spectrum pulse propagating through lossy media. If the sidelobes are considered, the usable bandwidth is large. For a given target material, greater frequency downshift can be expected for higher order sidelobes. Therefore, this model can improve the spectral shift resolution compared to a Gaussian pulse.

An alternate approach to arrive at the spectral downshift is to utilize time domain measurements of the zero-crossing frequency of the rf signal. The relationship between the zero crossing frequency and the spectral power density of the signal was investigated by Rice [63] and Papoulis [64]. Flax et al. [65-66] applied this method to estimate the tissue attenuation and Narayana et al. [67] extended this technique to nonlinear attenuation with

frequency. Shaffer et al. [68] relaxed the Gaussian spectrum signal requirement. However, their techniques required knowledge of the parameter n, four moments of the power spectral density and the derivative of the mean frequency with respect to depth.

## IV.2 Evaluation of multi-layered material properties by spectral shift techniques

Consider a multi-layered structure with frequency-dependent attenuation (linear dependency and square law dependency) as shown in Figure IV.1, where  $H_i(f)$ ,  $r_i$  and  $D_i$  are the transfer function, the reflection coefficient and the layer thickness of the *i-th* layer media, respectively. The magnitude of the transfer function,  $|H_i(f)|$ , can be characterized by:

$$|H_i(f)| = exp(-\alpha f^n D_i)$$
 (i=1,....,N) (IV.2.1)

where

 $\alpha_i$ =attenuation coefficient of the *i-th* layer.

n =exponent of frequency dependency.

 $D_i$ = the thickness of the *i-th* layer.

f = frequency.

In order to simplify the analysis, the following assumptions are made:

- (1.) The incident signal has a Gaussian-shaped spectrum.
- (2.) The object under investigation consists of parallel homogeneous layers with the incident signal normal to the boundaries.
- (3.) Wave propagation through the medium is a linear time-invariant process.
- (4.) The thickness of layers is large compared to the incident pulse width to avoid signal overlapping.
- (5.) Higher order multiple reflections can be ignored (or eliminated by suitable gating).
- (6.) The attenuation of the coupling medium (usually water) is considered to be zero.

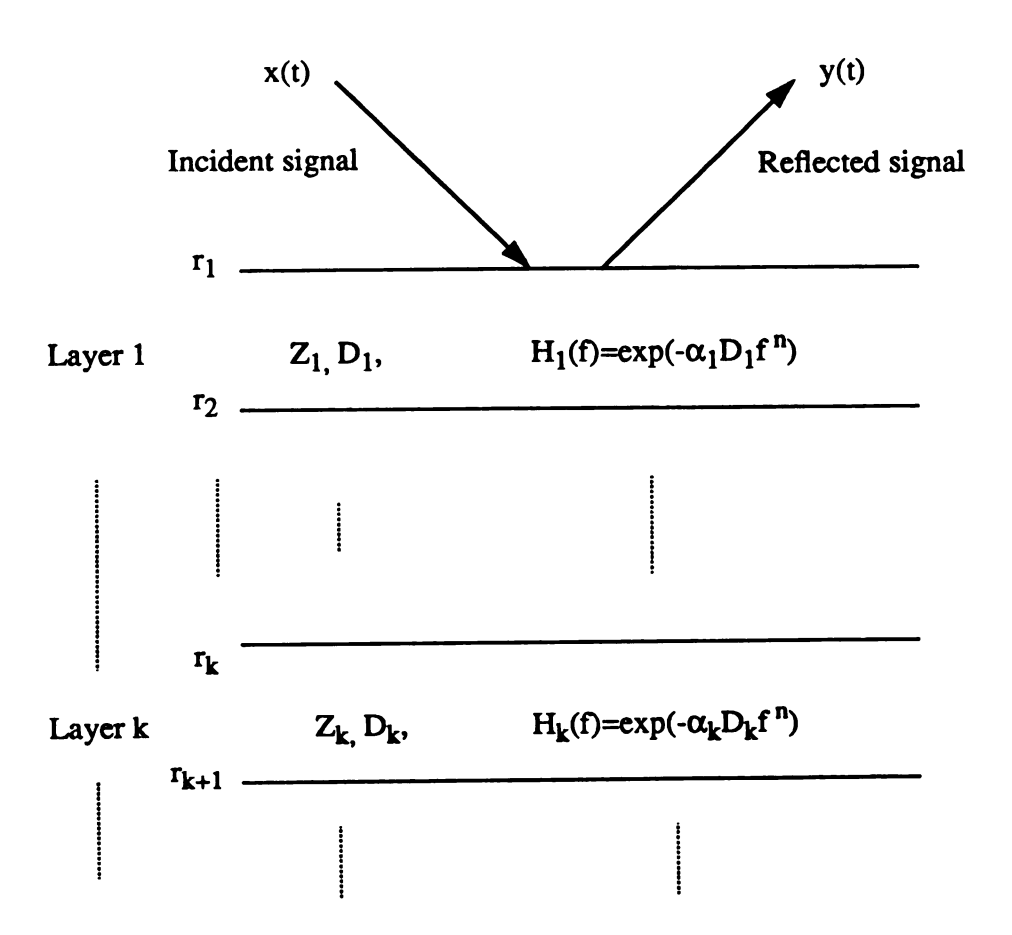


Figure IV.1 Multi-layered medium model.

In order to have a Gaussian-shaped spectrum in the frequency domain of the incident pulse, we choose the incident pulse in the time domain as follows:

$$x(t) = exp\left(-\frac{t^2}{2\sigma_0^2}\right)\sin\left(2\pi f_0 t\right)$$
 (IV.2.2)

where

 $f_0$  = the center frequency

 $\sigma_0$  = the standard deviation of the Gaussian-shaped envelope.

The toneburst duration of x(t) is approximately equal to  $6\sigma_0$ . The range resolution, in the time domain, is determined by the selection of  $\sigma_0$ .

The Gaussian-shaped spectrum of the incident pulse, X(f), and its magnitude can be expressed as:

$$|X(f)| = \left| \int_{-\infty}^{\infty} x(t) e^{-j2\pi f t} dt \right| = ce^{-\frac{(f-f_0)^2}{2\sigma_f^2}}$$
(IV.2.3)

where

$$c = \sqrt{2\pi}\sigma_0$$
 is a constant 
$$\sigma_f^2 = 1/(4\pi^2\sigma_0^2)$$
 is the variance.

Therefore, the half amplitude bandwidth, B for X(f) in (IV.2.3) can be expressed as:

$$B = 2.357 \cdot \sigma_f = \frac{0.589}{\pi \sigma_0} \tag{IV.2.4}$$

After the pulse propagates through the multi-layered structure and echoes back from each boundary, we can use a variable window size and location to gate a nonoverlapped sequence of pulses  $(y_1(t), y_2(t), \dots, y_{N+1}(t))$  from the return signal, y(t), as shown in *Figure* IV.2. The window size should be larger than the toneburst duration of the nonoverlapped echoes. The rectangular window is centered at each nonoverlapped pulse.

By transforming each gated pulse into the frequency domain by some FFT (Fast Fourier Transform) algorithm,  $Y_i(f)$ , (i=1,....,N+1), the magnitude for each gated signal can be expressed as following:

$$|Y_1(f)| = |X(f)||r_1|$$

and

$$|Y_{i+1}(f)| = |X(f)||A_{i+1}(r_1...r_{i+1})|\prod_{k=1}^{i}|H_k(f)|^2$$
 (i=1,....,N) (IV.2.5)

where  $A_{i+1}(r_1, \dots, r_{i+1})$  is defined as the reflectivity function and expressed as:

$$A_{i+1}(r_1...r_{i+1}) = r_{i+1} \prod_{k=1}^{i} (1-r_k^2)$$
 (i=1,....,N). (IV.2.6)

If we substitute equations (IV.2.1) and (IV.2.3) into equation (IV.2.5), we obtain the following spectral magnitude of gated pulses:

$$|Y_1(f)| = |X(f)||r_1|$$

and

$$|Y_{i+1}(f)| = |X(f)||A_{i+1}(r_1...r_{i+1})|\prod_{k=1}^{i} e^{-2\alpha_k D_k f^k}$$
 (i=1,....,N) (IV.2.7)

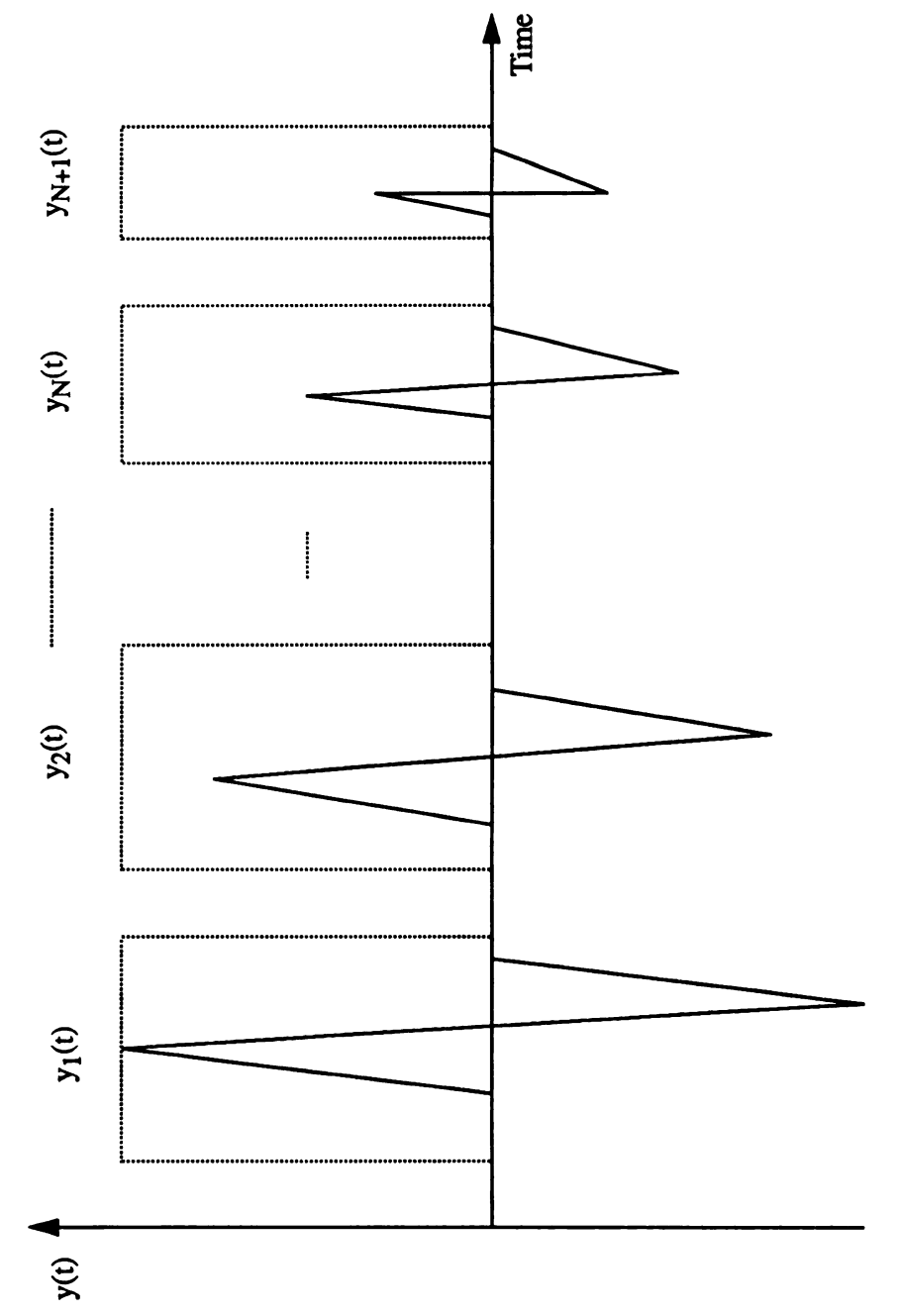


Figure IV.2 Reflected signal gating by a variable window to obtain a sequence of pulses.

Consider the following cases:

### CASE I. Linear frequency-dependent attenuation (n=1).

The pulse spectrum from the (i+1) th interface can be found from:

$$|Y_{i+1}(f)| = C_{i+1}|A_{i+1}|e^{-\frac{(f-f_{i+1})^2}{2\sigma_f^2}}$$
 (i=1,....,N) (IV.2.8)

with  $f_1 = f_0$  (assuming the coupling medium has no attenuation),

$$f_{i+1} = f_0 - 2\sigma_f^2 \sum_{k=1}^{i} \alpha_k D_k$$
 (i=1,....,N)

 $C_{i+1}$  a constant and independent of frequency, and  $A_{i+1}$  is given in equation (IV.2.6). Observing equation (IV.2.8), we find that the gated pulse spectrum maintains the same Gaussian shape form as that of the incident pulse, with the same standard deviation, but down shifted in center frequency.

From equation (IV.2.9), the center frequency difference,  $\Delta f_i$ , between two successive gated pulses is defined as:

$$\Delta f_i = f_{i+1} - f_i = 2\sigma_f^2 \alpha_i D_i = \frac{1}{2\pi^2 \sigma_0^2} \alpha_i D_i$$
 (i=1,....,N)

Observing equation (IV.2.10), we find that the downshifted center frequency difference is proportional to the bandwidth of the incident signal. Therefore, a larger bandwidth signal has not only good range resolution in the time domain but also good resolution in the

frequency domain. This is the reason to choose broadband signals for frequency domain interrogation.

The attenuation coefficient of the i-th layer,  $\alpha_i$ , is obtained from equation (IV.2.10) and given by:

$$\alpha_i = \frac{\Delta f_i}{2\sigma_f^2 D_i} = \frac{2\pi^2 \sigma_0^2 \Delta f_i}{D_i}$$
 (i=1,...,N) (IV.2.11)

As the pulse propagates through a medium with linear frequency-dependent attenuation, its spectrum is not only down-shifted in center frequency, but its amplitude is attenuated as well, as shown exaggerated in *Figure IV.3*. The peak spectral amplitude,  $p_i$ , of the *i-th* gated pulse at center frequency  $f_i$  can be obtained as follows:

The peak spectral amplitude of the first gated pulse,  $p_1$ , is

$$p_1 = |X(f_1)| |r_1|$$

and the (i+1)th peak spectral amplitude,  $p_{i+1}$ , is

$$p_{i+1} = |Y_{i+1}(f_{i+1})|$$

$$= |X(f_{i+1})||A_{i+1}|\prod_{k=1}^{i}|H_k(f_{i+1})|^2 \qquad (i=1,...,N)$$
 (IV.2.12)

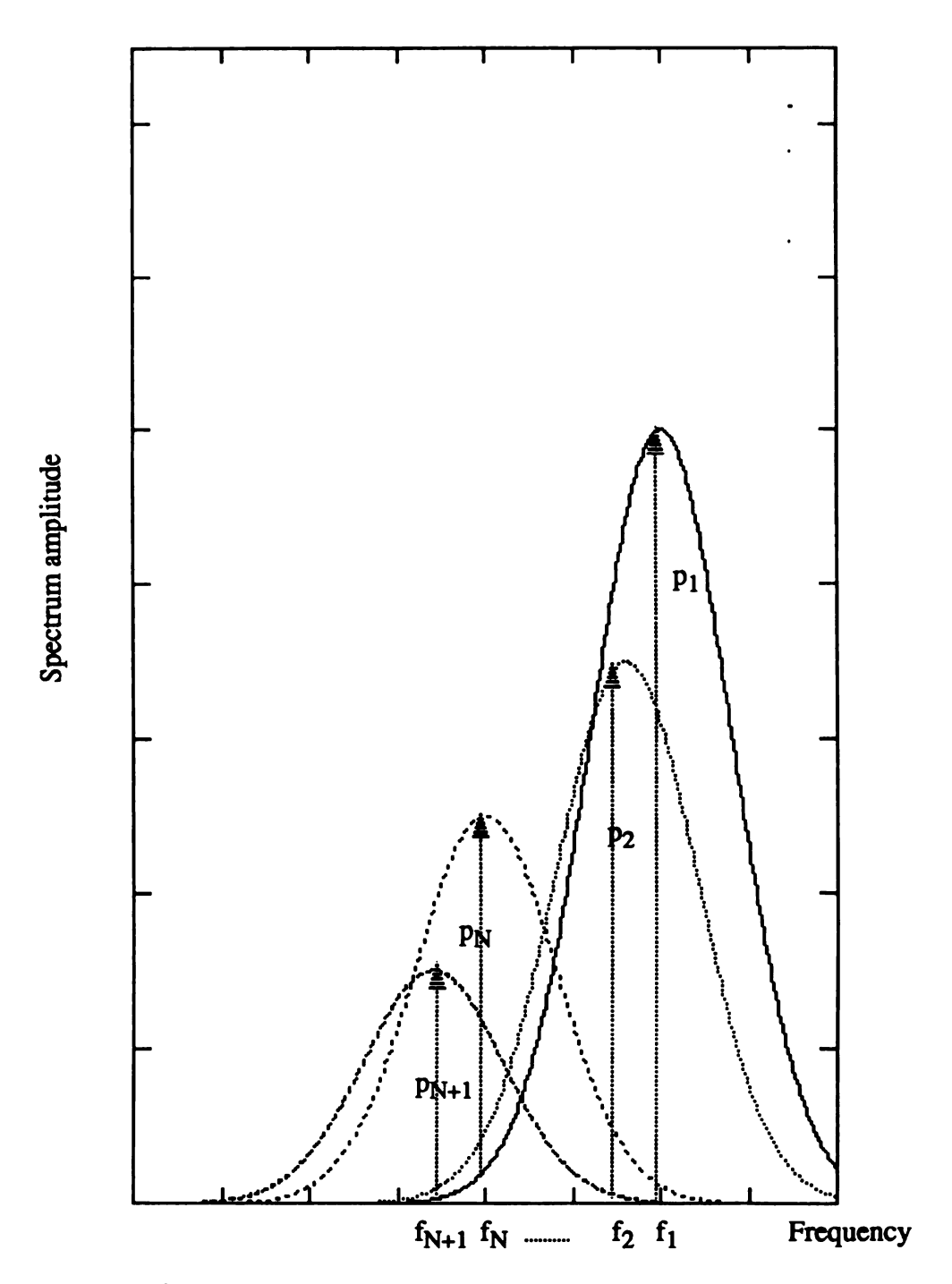


Figure IV.3 The downshift in center frequency and amplitude reduction for sequential gated pulses.

The amplitude ratio of successive gated pulses can then be expressed as:

$$\frac{p_{i+1}}{p_i} = \frac{|X(f_{i+1})||A_{i+1}| \prod_{k=1}^{i} |H_k(f_{i+1})|^2}{|X(f_i)||A_i| \prod_{k=1}^{i-1} |H_k(f_i)|^2}$$

$$= \frac{\left|X(f_{i+1})\right| \prod_{k=1}^{i} |H_k(f_{i+1})|^2}{\left|X(f_i)\right| \prod_{k=1}^{i-1} |H_k(f_i)|^2} \cdot \left|\frac{r_{i+1}(1-r_i^2)}{r_i}\right| \qquad (i=1,....,N) \quad (IV.2.13)$$

We observe from equation (IV2.13) that the left hand side is a known quantity which is measured experimentally. Once, the  $\alpha_i$ , are determined from equation (IV.2.11), the right hand side of equation (IV.2.13) can be calculated except for  $r_{i+1}$  and  $r_i$ . If the reflection coefficient,  $r_1$ , at the first boundary is known ( $r_1$  can be measured by a simple experimental setup such as shown in *Figure* IV.4), the successive reflection coefficients,  $r_2$ ,  $r_3$ ,...... $r_{N+1}$ , can be evaluated iteratively, from equation (IV.2.13):

$$|r_{i+1}| = \frac{|r_i|}{(1-r_i^2)} \cdot \frac{p_{i+1}}{p_i} \cdot \frac{|X(f_i)| \prod_{k=1}^{i-1} |H_k(f_i)|^2}{|X(f_{i+1})| \prod_{k=1}^{i} |H_k(f_{i+1})|^2}$$
 (i=1,...,N) (IV.2.14)

The sign of  $r_{i+1}$  is determined by the same method as described in the previous chapter. Once the reflection coefficients,  $r_i$ , are determined, the acoustic impedance can be obtained by the following relationship:

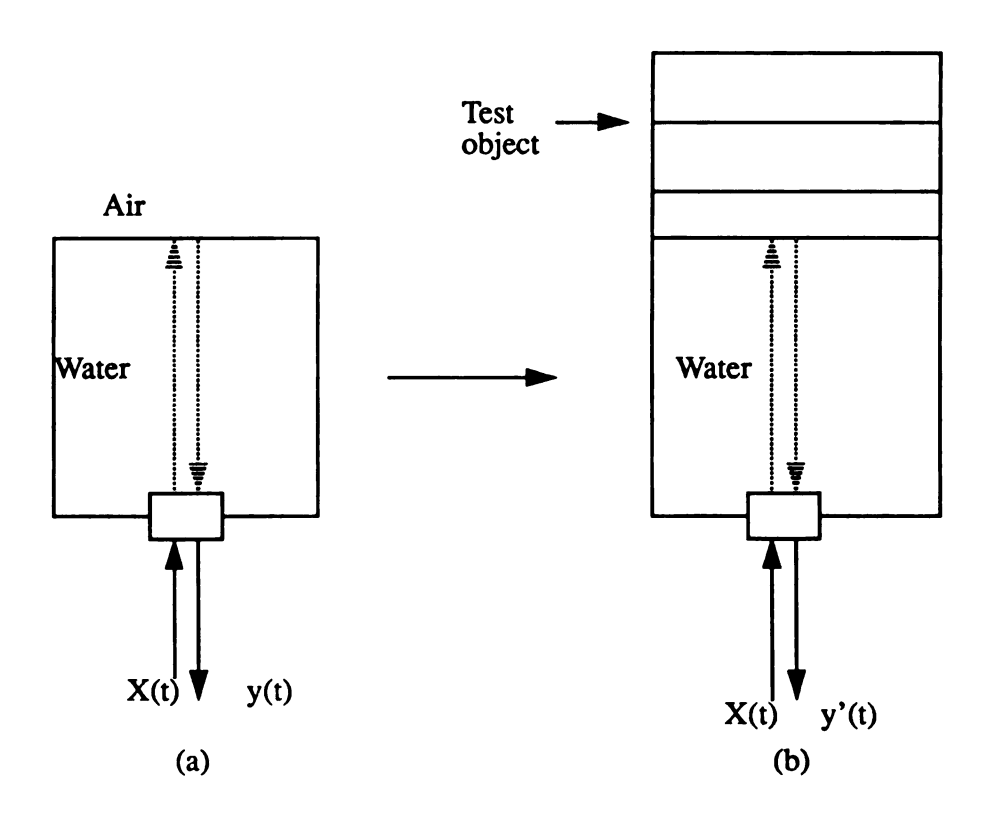


Figure IV.4 Schematic for measuring r<sub>1</sub>.

$$Z_i = Z_{i-1} \cdot \frac{1+r_i}{1-r_i}$$
 (i=1,....,N) (IV.2.15)

Since the acoustic impedance,  $Z_0$ , of the coupling media (usually water) is a known quantity, the acoustic impedance,  $Z_i$ , for each layer can be obtained.

#### CASE II. Quadratic frequency-dependent attenuation (n=2):

By substituting  $H_i(f) = exp(-2\alpha_i f^2 D_i)$  into equation (IV.2.7) we obtain the following relationships:

$$|Y_1(f)| = |r_1||X(f)|$$

and

$$|Y_{i+1}(f)| = C_{i+1}|A_{i+1}|e^{-(f-f_{i+1})^2/(2\sigma_{i+1}^2)}$$
 (i=1,....,N) (IV.2.16)

where  $C_{i+1}$  is constant and independent of frequency,  $A_{i+1}$  is the same as given in equation (IV.2.6). Since the wave through the coupling medium has no down-shift in center frequency, the center frequencies and standard deviation of the i-th gated signal are:

$$f_1 = f_0$$

and

$$f_{i+1} = \frac{f_0}{1 + 4\sigma_f^2 \sum_{k=1}^{i} \alpha_k D_k}$$
 (i=1,....,N)

and

$$\sigma_{i+1}^2 = \frac{\sigma_f^2}{1 + 4\sigma_f^2 \sum_{k}^{i} \alpha_k D_k}$$
 (i=1....,N) (IV.2.18)

Judging from equations (IV.2.16)-(IV.2.18), we find that the spectrum of the gated pulses remains Gaussian with a down-shifted center frequency. The spectral bandwidth becomes narrower since the standard deviation is less than that of the previous pulses. Denoting the ratio of center frequencies by  $F_i$ , we obtain:

$$F_{i+1} = \frac{f_0}{f_{i+1}} = 1 + 4\sigma_f^2 \sum_{k=1}^{i} \alpha_k D_k$$
 (i=1,...,N) (IV.2.19)

The spectral ratio difference,  $\Delta F_i$ , is then:

$$\Delta F_{i} = F_{i+1} - F_{i} = 4\sigma_{f}^{2}\alpha_{i}D_{i}$$

$$= \frac{\alpha_{i}D_{i}}{\pi^{2}\sigma_{0}^{2}} \qquad (i=1,....,N)$$
(IV.2.20)

The attenuation coefficient,  $\alpha_i$ , is found to be:

$$\alpha_i = \frac{\Delta F_i}{4\sigma_f^2 D_i} = \frac{\pi^2 \sigma_0^2 \Delta F_i}{2D_i}$$
 (i=1,....,N)

Once the individual attenuation coefficient,  $\alpha_i$  are determined, the reflection coefficients  $r_i$  can be calculated from equation (IV.2.14). Therefore, the acoustic impedances,  $Z_i$  (i=1,...,N), can be calculated from equation (IV.2.15).

In summary, the following procedure can be used to find the attenuation coefficients and acoustic impedances of multi-layered structures:

- (1.) Obtain a series of gated pulses from the echo return by using appropriate window widths.
- (2.) Transform these gated pulses into the frequency domain. The attenuation property (i.e. n=1 or n=2) can be determined by comparing the standard deviation of the successive gated pulse spectra. If the standard deviation of successive gated pulses remain unchanged, one can conclude that the attenuation is linear frequency-dependent and the value n=1 should be used. The attenuation coefficient is then evaluated by the technique outlined for case I. If the standard deviation is less than that of the previous gated pulse, the square-law dependent model (n=2) should be used. The attenuation is calculated by using the method employed in case II.
- (3) The reflection coefficient,  $r_1$ , at the first interface, can be obtained experimentally as suggested in *Figure* IV.4. In practice, it is rather difficult to get a replica of the incident pulse from the transmitter/receiver transducer. Experimentally, the incident pulse x(t) can be obtained from the water/air reflection as shown in *Figure* III.3(a) which is used to compare with the amplitude of the echo return signal from *Figure* III.3(b) to determine  $r_1$ . Finally, the remaining reflection coefficients can be computed iteratively from equation (IV.2.14).

#### IV.3. Evaluation of nonlinear attenuation parameters.

The formulation of the previous section is only valid for the cases of n=1 and n=2. Many researchers [68-71] were shown that the frequency dependency of attenuation n for most biological tissue is between 1 and 2. (i.e. 1 < n < 2). Although most attenuation estimation methods are based on the assumption that tissue attenuation is linearly frequency dependent, for nonlinear attenuation, such methods could produce biased results. In this section, we intend to utilize the spectral shift technique to estimate the parameter n. In general, the transfer function of the attenuation process can be characterized by:

$$|H(f)| = exp(-2\alpha f^{\prime}D)$$
 (IV.3.1)

where

 $\alpha$  = attenuation coefficient.

n = exponent of frequency dependency (typically,  $1 \le n \le 2$ ).

D = propagating distance.

f = frequency.

We can utilize the Taylor expansion to expand  $f^n$  about the center frequency  $f_0 = 2.25$  MHz as follows:

$$f^{n} = f_{0}^{n} + n f_{0}^{n-1} (f - f_{0}) + \frac{n(n-1)}{2!} f_{0}^{n-2} (f - f_{0})^{2} + \dots$$
 (IV.3.2)

If the bandwidth of the interrogating signal is within 2.0 MHz at 2.25 MHz center frequency, we can obtain the following approximation from equation (IV.3.2).

$$f^{n} \approx f_{0}^{n} + n f_{0}^{n-1} (f - f_{0}) + \frac{n(n-1)}{2!} f_{0}^{n-2} (f - f_{0})^{2}$$
 (IV.3.3)

The approximation error for n=1.2,n=1.5, and n=1.8 with  $1.75MHZ \le f \le 2.85MHZ$  is shown in Figure IV.5

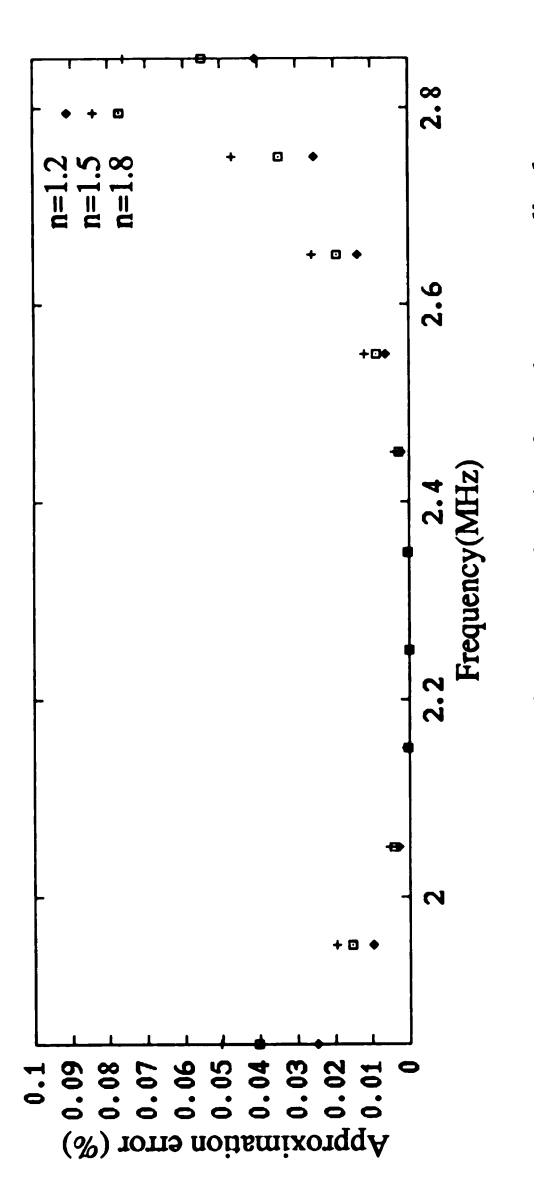


Figure IV.5 The deviation of the approximation from the true amplitude for different exponent dependencies.

From Figure IV.5, it is obvious that the narrower the bandwidth, the better the truncated Taylor series approximation. For an incident signal bandwidth of less than 2.0 MHz. The approximation limited to the quadratic term is appropriate. By substituting equation (IV.3.3) into equation (IV.3.1), the transfer function of the attenuation process can be expressed as:

$$|H(f)| = \exp(-\alpha D(n^2 - 3n + 2)f_0^n - 2n(2 - n)f_0^{n-1}\alpha Df - 2n(n - 1)f_0^{n-2}\alpha Df^2)$$
(IV.3.4)

Again assuming that the incident pulse has a Gaussian shaped spectrum given by:

$$|X(f)| = \frac{1}{\sqrt{2\pi}\sigma_0} exp\left(-\frac{(f-f_0)^2}{2\sigma_0^2}\right)$$
 (IV.3.5)

The output spectrum after passing through an arbitrary medium is, from equations (IV.3.4) and (IV.3.5), given by.

$$|Y(f)| = |X(f)| \cdot |H(f)| = \frac{1}{\sqrt{2\pi}\sigma_0} exp\left(-\frac{(f-f_0)^2}{2\sigma_0^2}\right).$$

$$exp(-\alpha D(n^2-3n+2)f_0^n-2n(2-n)f_0^{n-1}\alpha Df-2n(n-1)f_0^{n-2}\alpha Df^2)$$

$$= c \cdot exp\left(-\frac{(f - f_c)^2}{2\sigma_f^2}\right)$$
 (IV.3.6)

where

$$c = \frac{1}{\sqrt{2\pi}\sigma_0} \cdot exp \left[ 2 (n^2 - 4n - 2) f_0^n \sigma_0^2 \alpha D \right]$$

$$-\frac{(f_0 - 4n(2-n)f_0^{n-1}\sigma_0^2 \alpha D)^2}{1 + 2n(n-1)f_0^{n-2}\sigma_0^2 \alpha D}$$
,(IV.3.7)

$$f_c = \frac{f_0 - 2n(2 - n)f_0^{n - 1}\sigma_0^2 \alpha D}{1 + 2n(n - 1)f_0^{n - 2}\sigma_0^2 \alpha D}$$
,(IV.3.8)

and

$$\sigma_f^2 = \frac{\sigma_0^2}{1 + 2n(n-1)f_0^{n-2}\sigma_0^2 \alpha D} \qquad (IV.3.9)$$

From equation (IV.3.9), a variance ratio,  $r_{\sigma}$ , is given by:

$$r_{\sigma} = \frac{\sigma_0^2}{\sigma_f^2} = 1 + 2n(n-1)f_0^{n-2}\sigma_0^2\alpha D$$
 (IV.3.10)

The center frequency ratio,  $r_f$ , is given by:

$$r_f = \frac{f_0}{f_c} = \frac{1 + 2n(n-1)f_0^{n-2}\sigma_0^2 \alpha D}{1 - 2n(2-n)f_0^{n-2}\sigma_0^2 \alpha D}$$
(IV.3.11)

From equations (IV.3.10) and (IV.3.11), the exponent of frequency dependency, n, is as follows:

$$n = 1 + \frac{r_f(r_{\sigma} - 1)}{r_{\sigma}(r_f - 1)}$$
 (IV.3.12)

From the above equations, the parameter n is related to the variance ratio and to the center frequency ratio. Therefore, n can be estimated from the measured values of  $r_{\sigma}$  and  $r_{f}$  without information on the thickness, D, of the region of interest. This is fortunate since D cannot be measured directly from an A-mode echo sequence because a precise value for the mean sound velocity is unavailable. In general, the sound velocity of medium under investigation has an unknown value. If the thickness, D, is available, we can substitute the estimated n into equation (IV.3.10) and obtain the attenuation coefficient,  $\alpha$ :

$$\alpha = \frac{r_{\sigma} - 1}{2n(n-1)f_0^{n-2}\sigma_0^2 D}$$
 (IV.3.13)

# **CHAPTER V**

# EXPERIMENTAL SETUP AND RESULTS

## V.1 Time domain methods for material properties evaluation

In order to substantiate the theory developed in chapter III, a five-layer model was constructed as shown in Figure V.1. (Layers I, III and V are plexiglass with linear frequency-dependent attenuation [72], Layers II and IV are water with quadratic frequency-dependent attenuation [55]. The reasons for choosing this experimental model are (1.) it is easy to implement in the laboratory, (2.) we can employ the existing techniques to measure the properties of single layer material for reference in comparing to the results of multi-layered models, and (3.) thin layers give less error using time domain techniques than thick layers, as discussed in section III.4. The ultrasonic transducer (2.25MHz, Panametrics) was excited by a pulser / receiver (Panametrics 5052 PRX75). The reflected signal was sampled at a 20 MHz sampling rate by an 8-bit resolution A / D converter (Waag II). For the 2.25 MHz transducer, this rate is more than adequate to prevent significant spectral distortion

due to aliasing. The captured signals were averaged 50 times for the purpose of improving the signal-to-noise ratio. In general, the noise has zero mean so that the more signals that are averaged the lower the relative noise level will be. The received signals from the two sided transducers are shown in *Figure* V.2. The impulse responses of the test object were obtained by simply locating the positions and amplitudes of the peaks of the echo signals  $y_1(t)$  and  $y_2(t)$ . The processed impulse responses  $h_1(t)$  and  $h_2(t)$  are shown in *Figure* V. 3. From  $h_1(t)$  and  $h_2(t)$ , we can obtain  $a_i$ ,  $b_i$  and  $\tau_i$ , where  $a_i$  and  $b_i$  are the amplitudes of the impulse responses,  $\tau_i$  are the travel times within the i-th layer. Putting these experimental data  $(a_i, b_i$  and  $\tau_i)$  into the expressions developed in chapter III, we can determine the properties (attenuation coefficients,  $\alpha_i$ , and acoustic impedance,  $Z_i$ ) of the five-layer model.

In order to measure the acoustic properties (attenuation coefficient and acoustic impedance) of the sample, we established the experimental setup shown in *Figure* V. 4. The amplitudes of the returned signals have the following relationships:

$$A_1 = RA_0 e^{-2\alpha_0 D_0} (V.1)$$

$$A_2 = R(R^2 - 1)A_0e^{-2\alpha_0 D_0}e^{-2\alpha_1 d_1}$$
 (V.2)

$$B_1 = RA_0 e^{-2\alpha_0 D_0} (V.3)$$

$$B_2 = R(R^2 - 1) A_0 e^{-2\alpha_0 D_0} e^{-2\alpha_1 (d_1 + d_2)}$$
 (V.4)

where

 $A_0$  = incident pulse amplitude

 $\alpha_0$ = attenuation coefficient of coupling medium

D<sub>0</sub>= the distance between transducer and sample

R = reflection coefficient from the boundary between the coupling media and the sample

 $\alpha_1$ = attenuation coefficient of the sample

d<sub>1</sub>= width of the thin sample

 $d_1 + d_2 =$ width of the thick sample.

From equations (V.2) and (V.4), the attenuation coefficient of the sample can be determined by:

$$\alpha_1 = \frac{1}{2d_2} ln \left( \frac{A_2}{B_2} \right) \tag{V.5}$$

The reflection coefficient, R, at the coupling medium / sample interface is:

$$R = \sqrt{1 + \frac{A_2}{A_1} \cdot \left(\frac{A_2}{B_2}\right)^{\frac{d_1}{d_2}}} \tag{V.6}$$

Once the reflection coefficient is determined, and the acoustic impedance,  $Z_0$ , of the coupling material (usually water) is known, the acoustic impedance of the sample is given by:

$$Z_{sample} = Z_0 \cdot \frac{1+R}{1-R} \tag{V.7}$$

The received signals from the *Figure* V. 4 experimental configuration are shown in *Figure* V. 5. In general, it is difficult to measure the incident amplitude A<sub>i</sub> directly from the transmitter / receiver transducer. However, from equations (V.5) to (V.7), we find that it does not require the information of the incident amplitude to determine the attenuation

coefficient and the acoustic impedance of the sample. From Figure V.5, we can obtain  $A_1$ = 0.4125,  $A_2$ = -0.201,  $B_1$ = 0.4125 and  $B_2$ = -0.116. The thickness of samples are 3.2 mm and 5.9 mm respectively. Substituting these data into equation (V.5), we can obtain the attenuation coefficient of the sample as:

$$\alpha = \frac{1}{2 \cdot 0.27} \cdot ln \left( \frac{-0.201}{-0.116} \right) = 1.0 \quad \frac{np}{cm}$$

The reflection coefficient at the coupling medium / sample interface, can be obtained from equation (V.6):

$$R = \sqrt{1 + \frac{-0.201}{0.4125} \cdot (\frac{-0.201}{-0.116})^{0.32/0.27}} = 0.28$$

The acoustic impedance of the water coupling medium,  $Z_0$ , is assumed to be known, so that the acoustic impedance calculated from equation (V.7) is given as:

$$Z_{sample} = 1.5 \ x10^6 \cdot \frac{1 + 0.28}{1 - 0.28} = 2.67 \ x10^6 \ \frac{kg}{m^2 s}$$

The widths of the multi-layered experimental structures are: layer I ( $d_1$ =3.2 mm), layer II ( $d_2$ =3.0 mm), layer III ( $d_3$ =3.2 mm), layer IV ( $d_4$ = 3.1 mm) and layer V ( $d_5$ =5.9 mm). From the impulse responses of the two sided target shown in *Figure* V.3, we obtain the following numerical data:  $a_1$ =0.802,  $a_2$ =-0.572,  $a_3$ =0.508,  $a_4$ =-0.215,  $a_5$ =0.205, and  $a_6$ =-0.079;  $b_1$ =-0.057,  $b_2$ =0.125,  $b_3$ =-0.145,  $b_4$ =0.268,  $b_5$ =-0.301, and  $b_6$ =0.802. The travel times for each layer are:  $\tau_1$ =2.9  $\mu$ sec.,  $\tau_2$ =4.05  $\mu$ sec,  $\tau_3$ =2.85  $\mu$ sec,  $\tau_4$ =4.15  $\mu$ sec, and  $\tau_5$ =5.25  $\mu$ sec.

Putting these data  $(a_i, b_i, \tau_i)$  and  $(a_i)$  into the expression developed in section III.2, we can determine the attenuation, acoustic impedance and sound velocity profiles for multi-layered models. The experimental results are compared to the values obtained from single layer measurements as shown in *Figures* V.6 to V.8. If the thicknesses of multi-layered model are not available, we can only get the attenuation-velocity product profiles as shown in *Figure* V. 9.

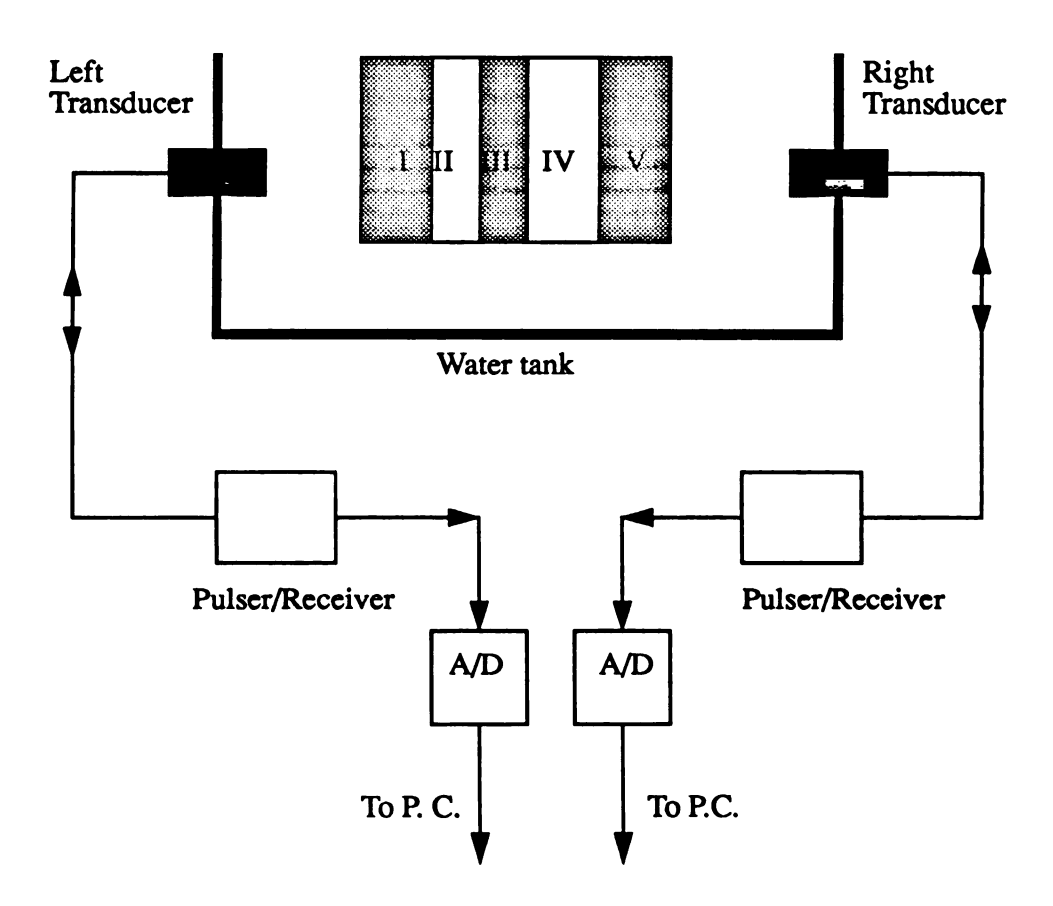
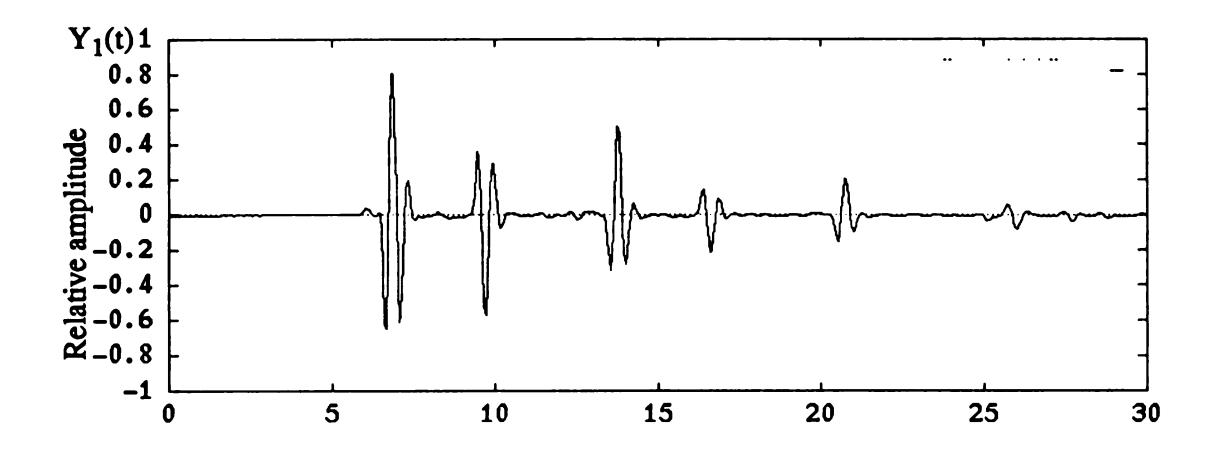


Figure V.1. Schematic for the experimental setup for time domain measurements.



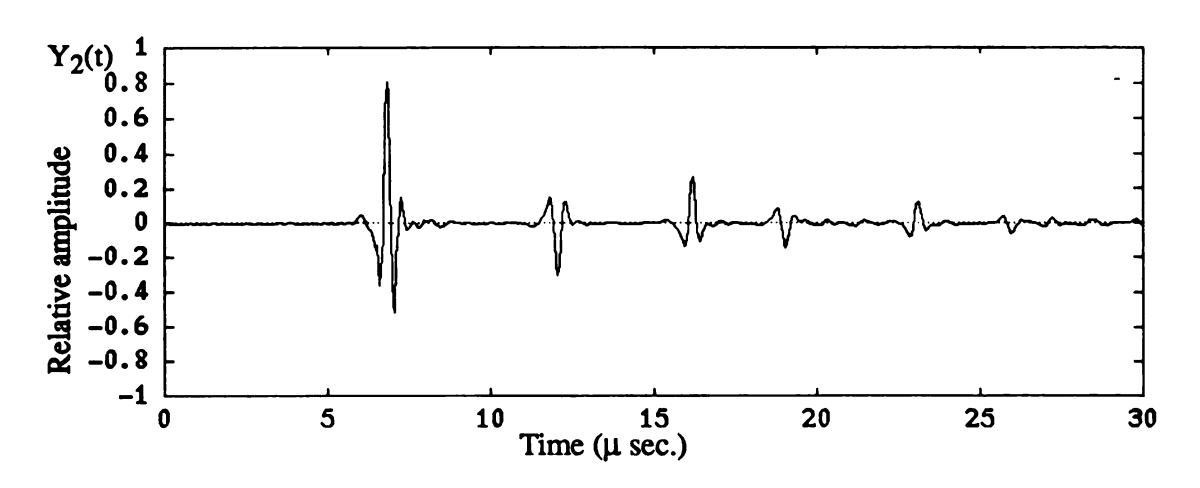
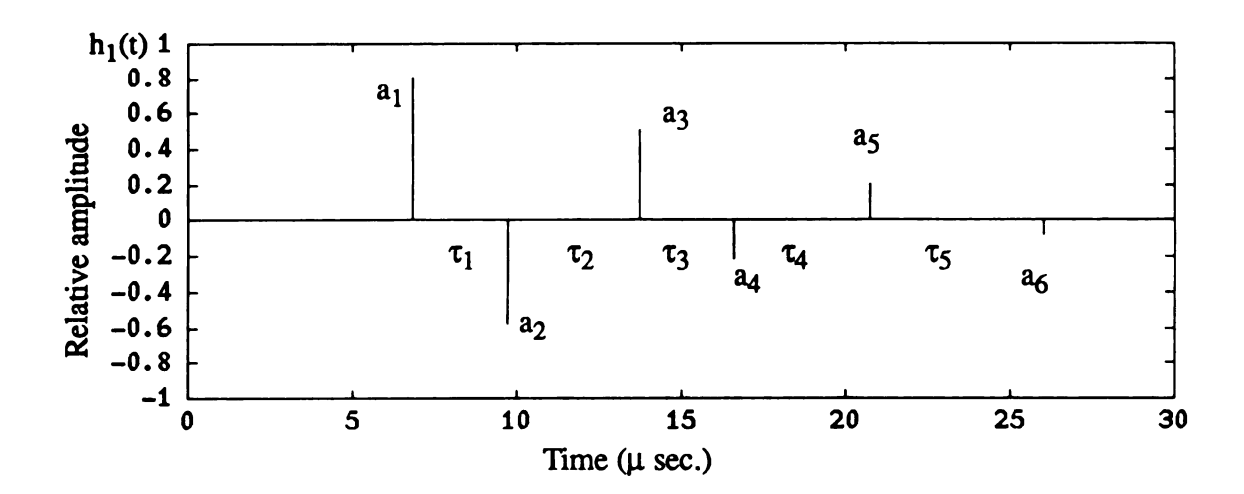


Figure V.2 Measured pulse echoes for dual interrogation.



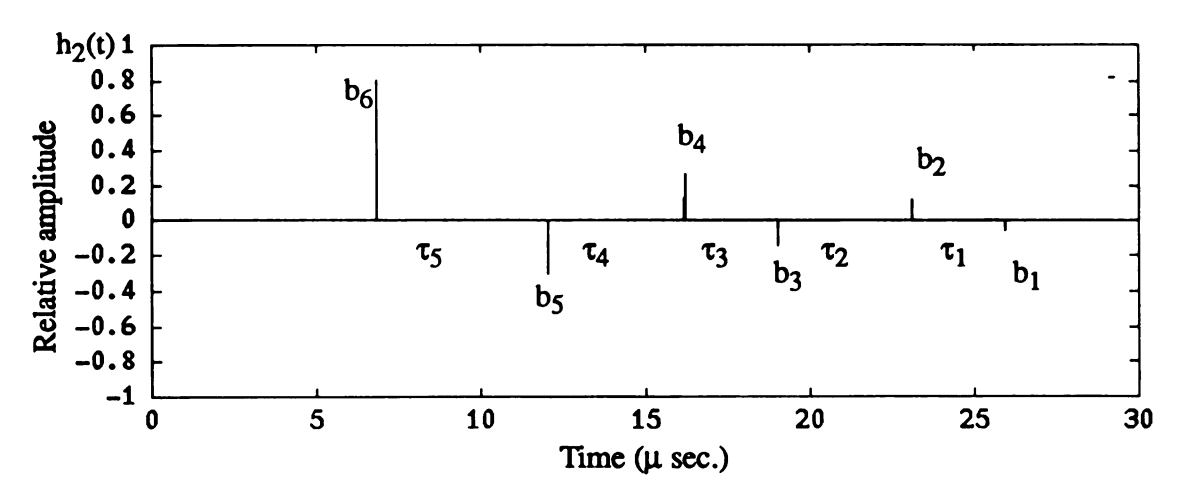


Figure V.3 Impulse responses of two sided interrogation.

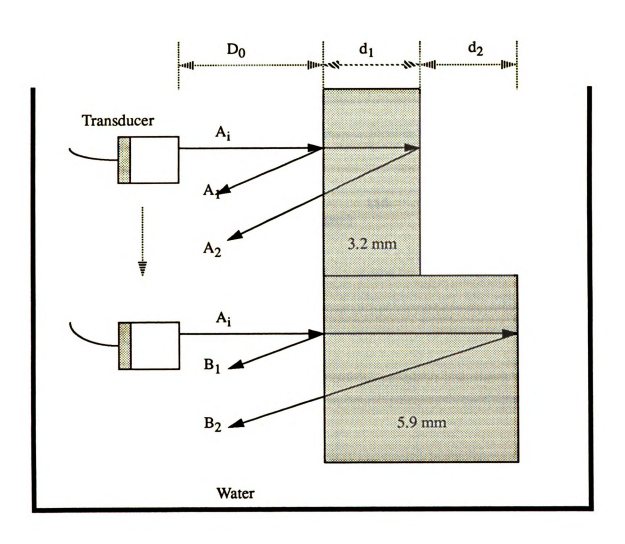
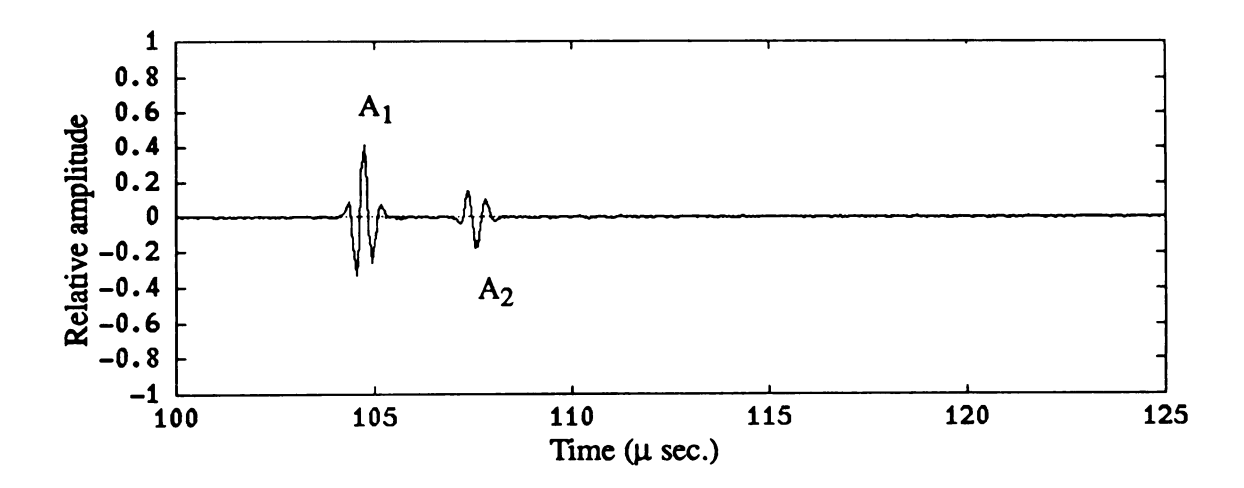


Figure V.4 Schematic for measuring sample properties.



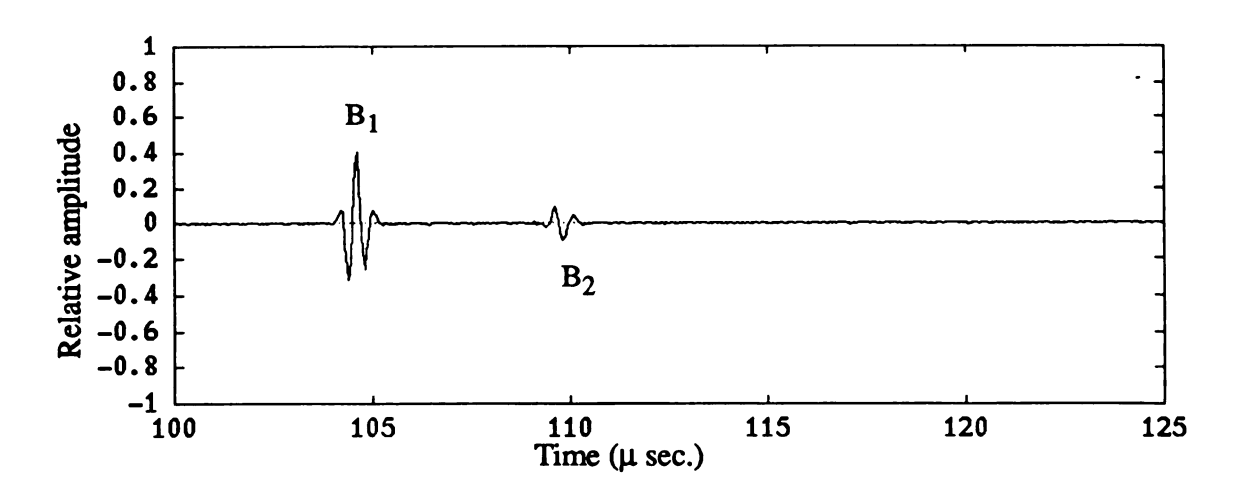


Figure V.5 The captured signals from Figure V.4 setup.

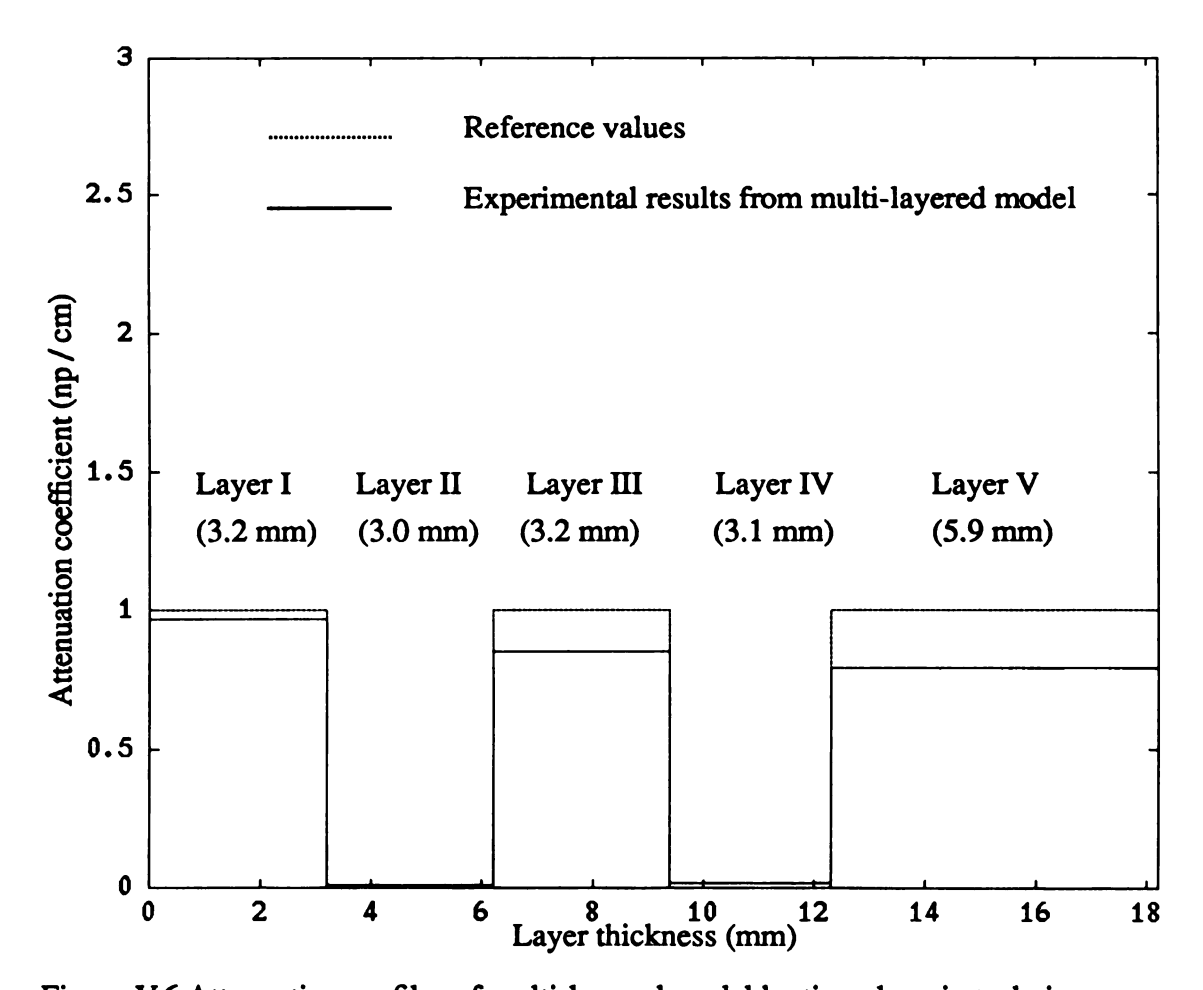


Figure V.6 Attenuation profiles of multi-layered model by time domain techniques.

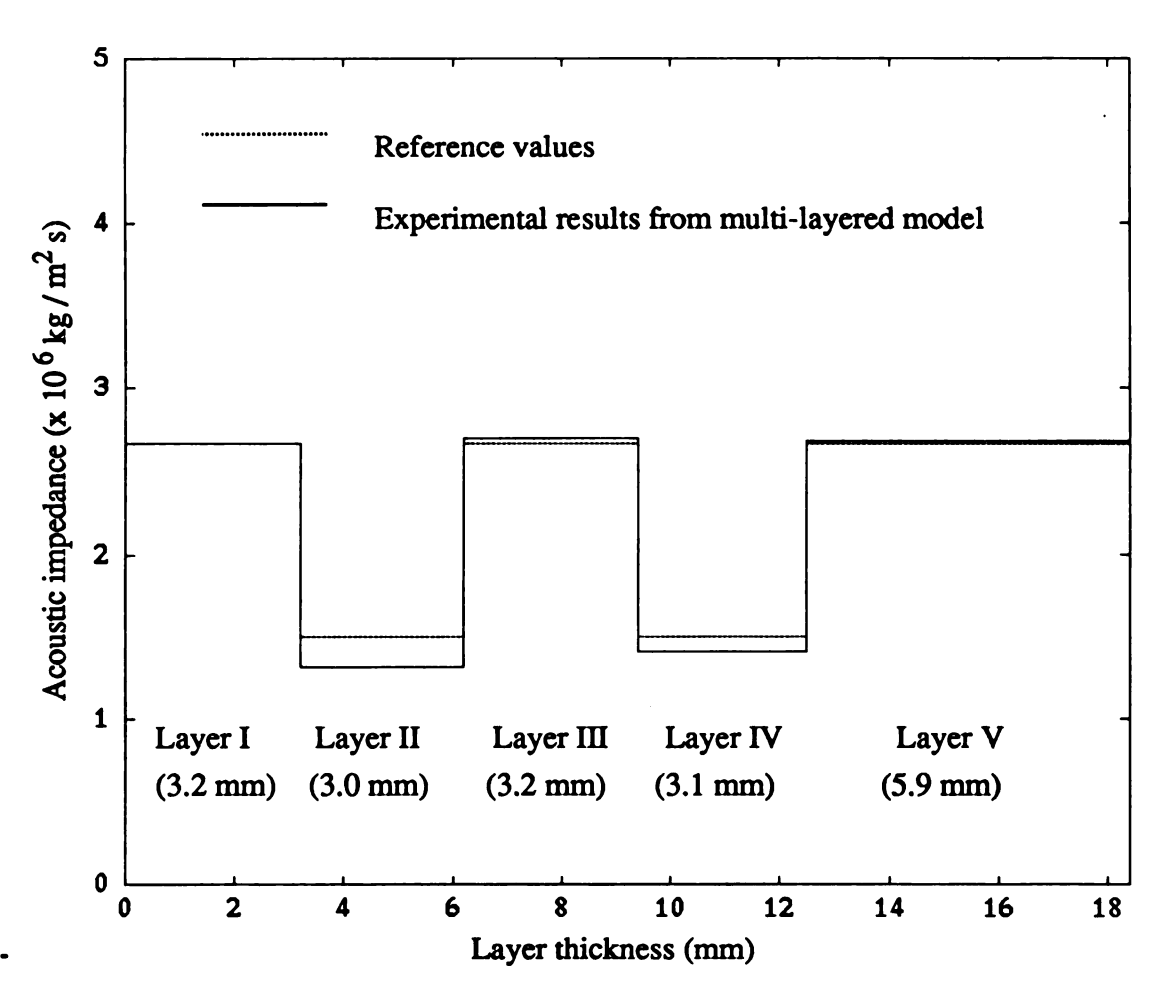


Figure V. 7 Acoustic impedance profiles of multi-layered model by time domain techniques.

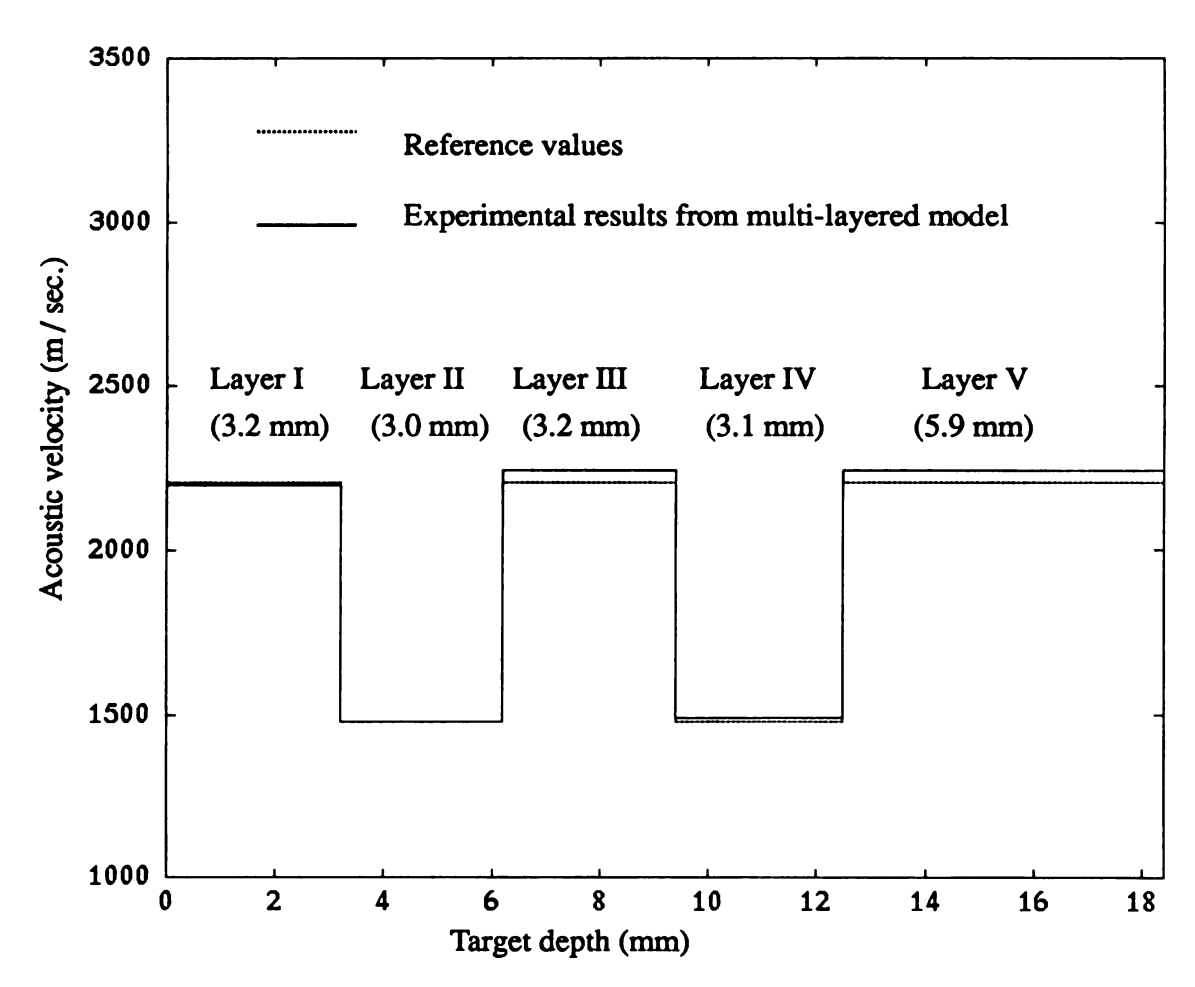


Figure V.8 Acoustic velocity profiles of multi-layered model by time domain techniques.

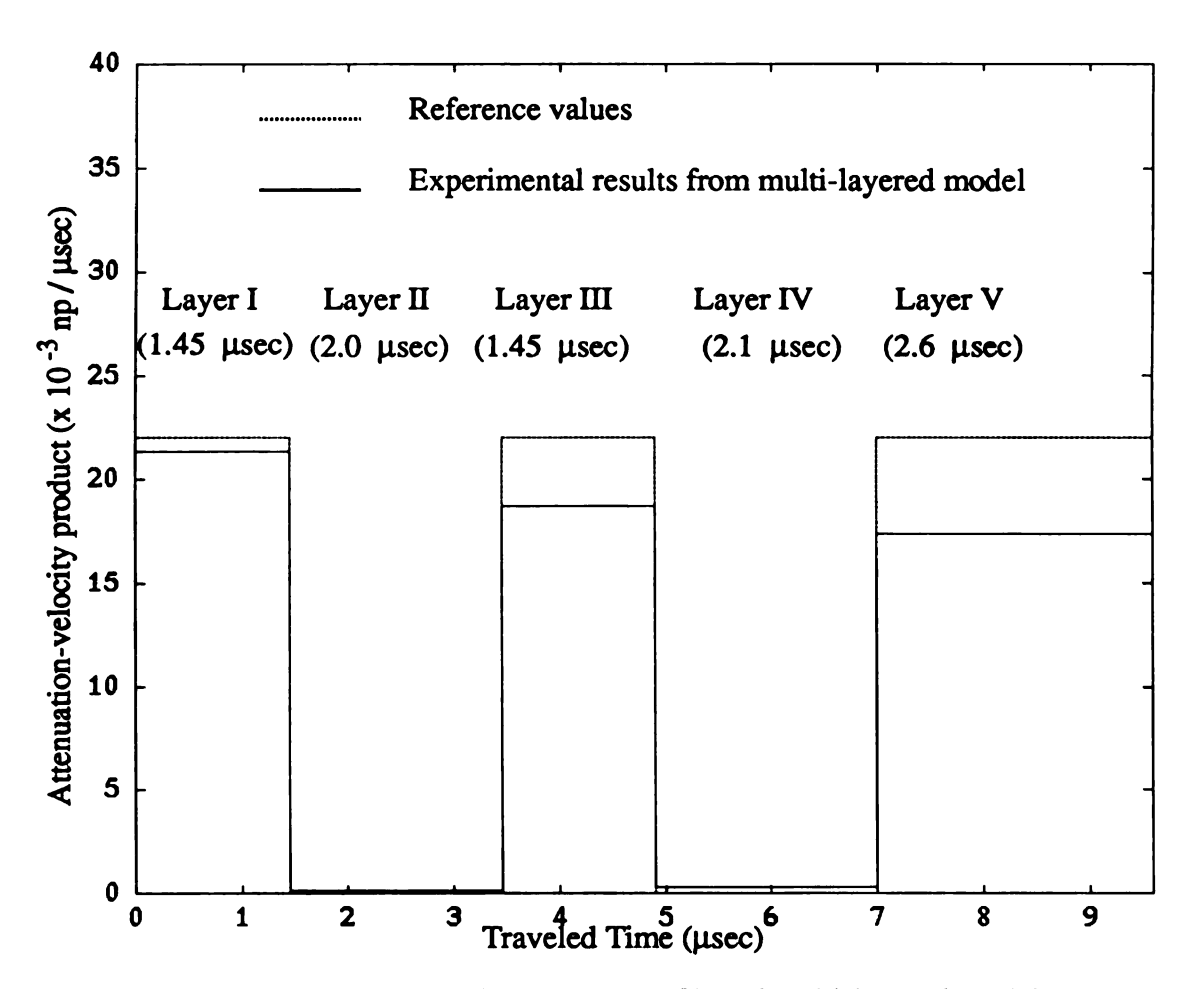


Figure V.9 Attenuation-velocity product profiles of multi-layered model by time domain techniques.

#### V.2 Frequency domain methods for material properties evaluation

In order to substantiate the spectral shift method developed in chapter IV, a three-layer model was constructed as shown in Figure V.10. The reason for choosing this experimental model are: (1.) the attenuation of plexiglass is linear frequency dependent (n=1) [72] while that of water is quadratic frequency dependent (n=2) [55], and (2.) thicker layers will generate a larger center frequency downshift which is easily measured in the frequency domain. The ultrasonic transducer, pulser/receiver unit and A/D converter are described in the previous section. Fifty captured received signals were averaged as shown in Figure V.11, to improve the signal-to-noise ratio. The received signals were gated by rectangular windows which are greater than the pulse widths of the incident signals in the time domain in order to preserve the spectral content of the signal. Therefore, a sequence of gated pulses,  $y_1(t)$ ,  $y_2(t)$ ,  $y_3(t)$  and  $y_4(t)$  were obtained as shown in Figure V.12. The gated pulses were zero padded to 1024-point signals as shown in Figure V.13 and transformed into the frequency domain, as shown in Figure V.14, using a decimation-in-time Fast Fourier Transform (FFT) program. The frequency resolution,  $\Delta f$ , is determined from the following relationship:

$$\Delta f = \frac{1}{NT} \tag{V.2.1}$$

where N is the number of samples and T is the sampling period. From our specification, N=1024, and  $T = \frac{1}{20x10^6}$  second (20 MHz sampling rate), so that  $\Delta f = 19.5$  kHz. There are two ways to increase frequency resolution namely to increase the number of samples or to reduce the sampling rate. However, the latter method will increase aliasing while the former will increase the computational complexity. In order to clearly see the downshifted center frequency, we plot the normalized spectra of the gated pulses as shown in

Figure V.15. The first moment formula to find the center frequency,  $f_i$ , given by:

$$f_{i} = \frac{\int_{f_{l}}^{f_{u}} f |H_{i}(f)| df}{\int_{f_{l}}^{f_{u}} |H_{i}(f)| df}$$
 (i=1,2,3,4)

where  $f_u$  and  $f_l$  are the upper and lower 3 dB cut-off frequencies of  $|H_i(f)|$ , was used to obtain the following center frequencies of the gated pulses:  $f_1$ =2.1289 MHz,  $f_2$ =1.9922 MHz,  $f_3$ =1.9726 MHz,  $f_4$ =1.6992 MHz. Since layer I and layer III are plexiglass with linear frequency dependent attenuation (n=1), we can use equation (IV.2.11) to calculate the attenuation coefficients as:

$$\alpha_1 = \frac{2\pi^2 \sigma_0^2 \Delta f_1}{D_1} = \frac{2\pi^2 (\frac{1.2}{6} \cdot 10^{-10})^2 (2.1289 - 1.9922) 10^6}{1.154}$$

$$= 0.0935 \frac{np}{cm \cdot MHz}$$

and

$$\alpha_3 = \frac{2\pi^2 \sigma_0^2 \Delta f_3}{D_3} = \frac{2\pi^2 (\frac{1.2}{6} \cdot 10^{-6})^2 (1.9726 - 1.6992) \cdot 10^6}{1.778}$$

$$= 0.1214 \frac{np}{cm \cdot MHz}$$

Layer II has a quadratic frequency dependent attenuation (n=2), so that we can utilize equation (IV.2.21) to calculate  $\alpha_2$ :

$$\alpha_2 = \frac{\pi^2 \sigma_0^2 \Delta f_2}{2D_2} = \frac{\pi^2 \left(\frac{1.2}{6} \cdot 10^{-6}\right)^2 \left(\frac{2.1289}{1.9726} - \frac{2.1289}{1.9922}\right)}{2 \cdot 1.125}$$
$$= 0.00172 \frac{np}{cm \cdot (MHz)^2}$$

Once the attenuation coefficients in each layer  $\alpha_1$ ,  $\alpha_2$  and  $\alpha_3$  have been determined, these values, along with  $r_1$ =0.38 and the spectral amplitude ratios  $\frac{p_{i+1}}{p_i}$ , can be substituted into equations (IV.2.13) and (IV.2.14) to determine the reflection coefficients,  $r_2$ =-0.32,  $r_3$ =0.30, and  $r_4$ =-0.28, respectively. These reflection coefficients can be used to obtain the acoustic impedances from the relationship:

$$Z_i = \frac{1+r_i}{1-r_i} \cdot Z_{i-1}$$
 (i=1,2,3)

From the known acoustic impedance of the water coupling medium,  $Z_0=1.5 \times 10^6$  kg/m<sup>2</sup>s, we can successively calculate the acoustic impedance for each layer giving:  $Z_1=3.34 \times 10^6$  kg/m<sup>2</sup>s,  $Z_2=1.72 \times 10^6$  kg/m<sup>2</sup>s and  $Z_3=3.19 \times 10^6$  kg/m<sup>2</sup>s. The acoustic impedance and attenuation coefficient profiles and compared with the published data [71-72] as shown in Figures V.16 and V.17. The results demonstrate the adequacy of the spectral shift technique. The worst case deviation occurs for layer III in Figure V.16 which shows an error of 13% from the published value. The discrepancies is due to the signal degradation in the deeper layers. In addition, the signal to noise for the third layer medium from the experimental apparatus employed approaches minimum acceptable level. Improvement in measurements would certainly result if higher quality instrumentation were available.

Nonetheless the experimental results were very encouraging.

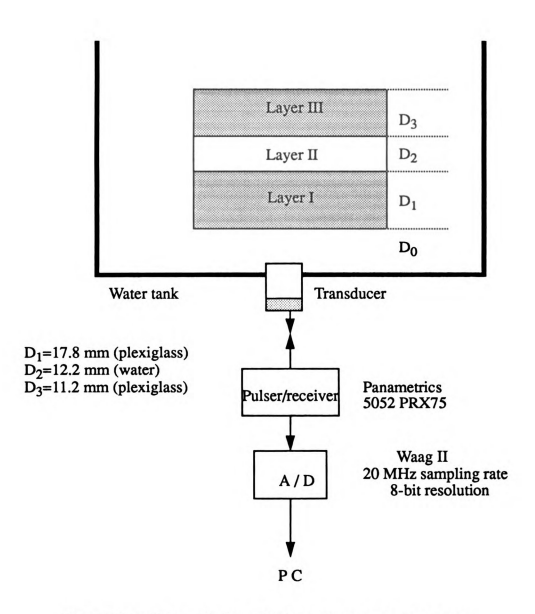


Figure V.10 Schematic for multi-layered target measurements.

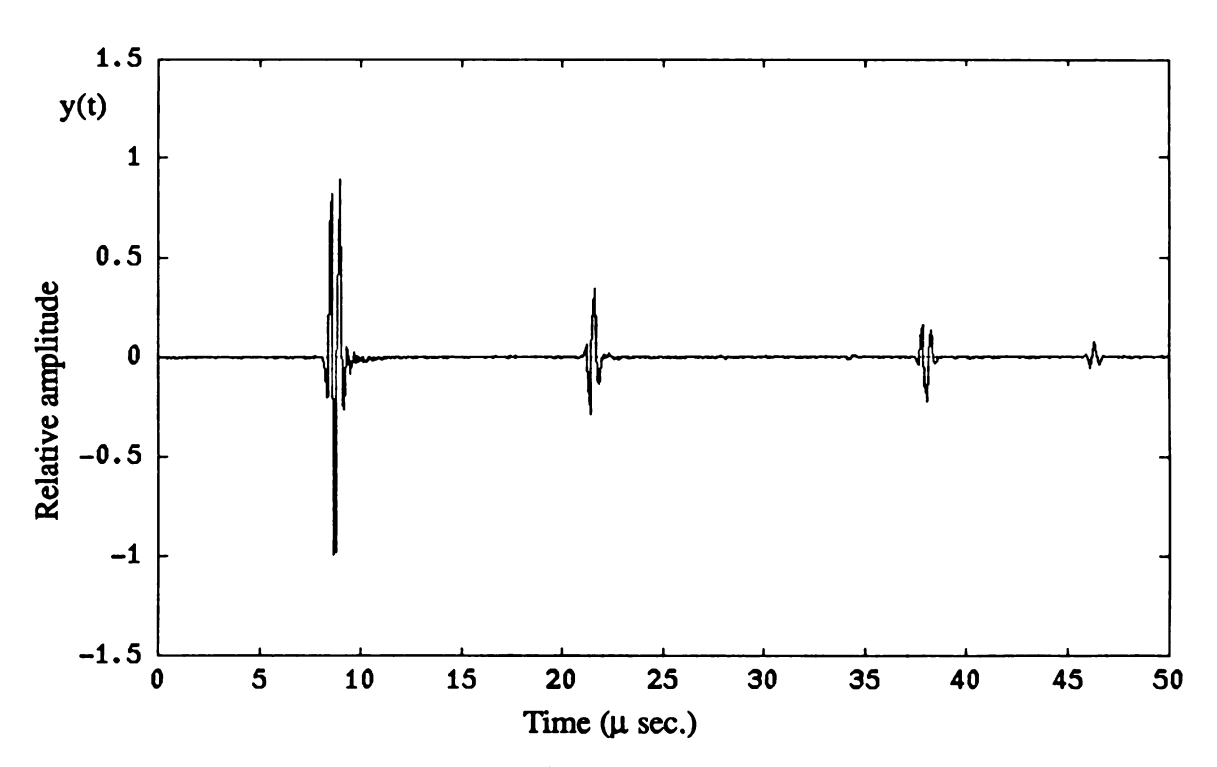


Figure V.11 The captured signals from a one sided multi-layered structure.

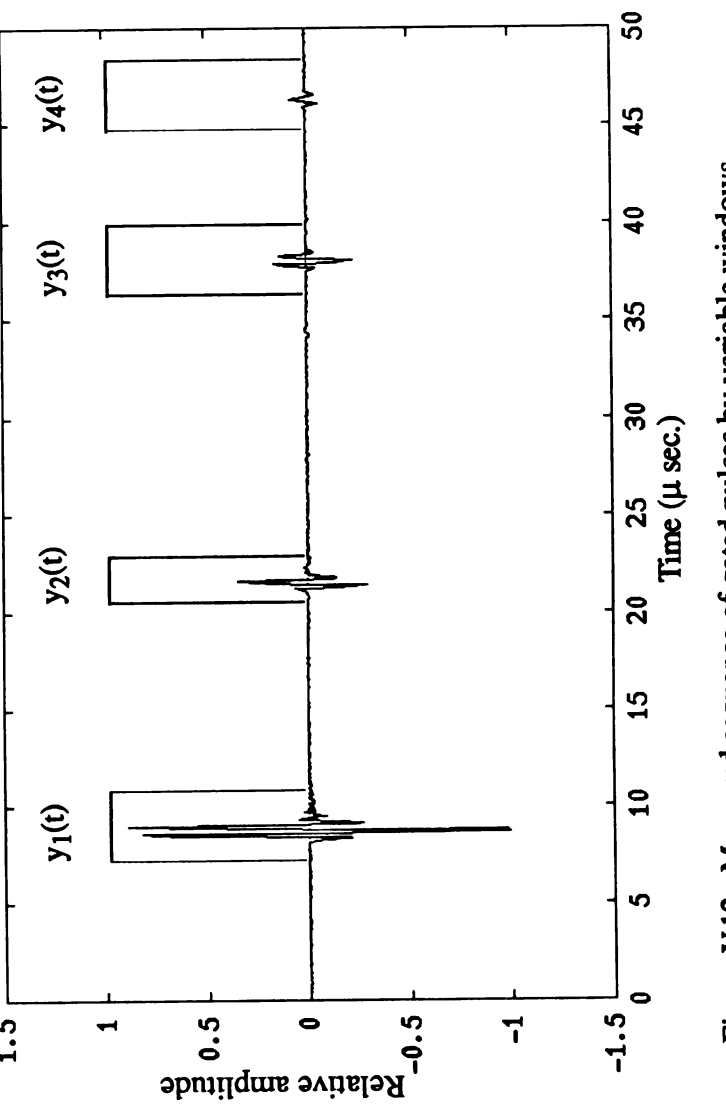
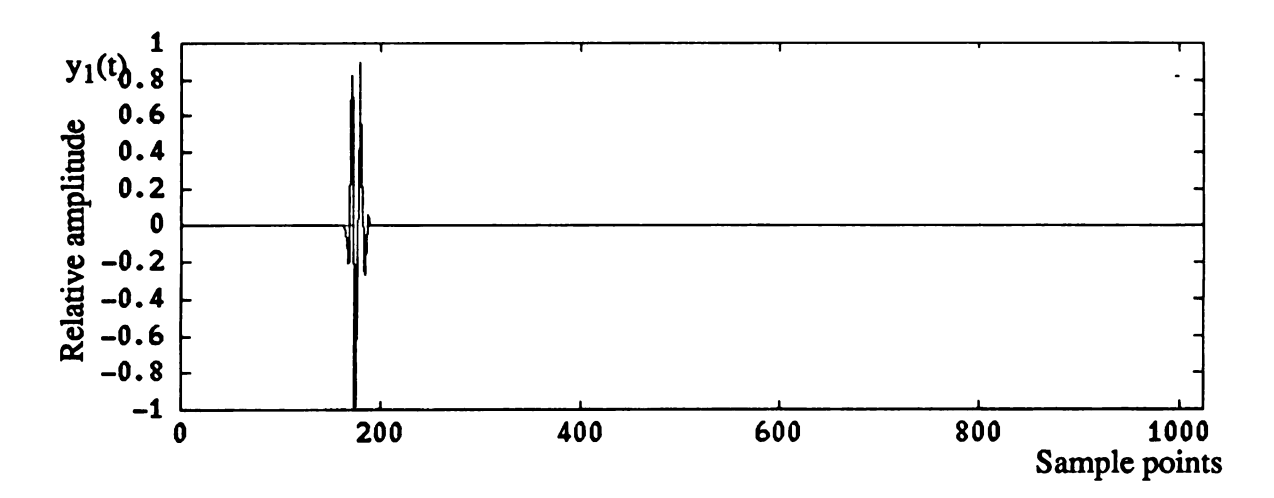
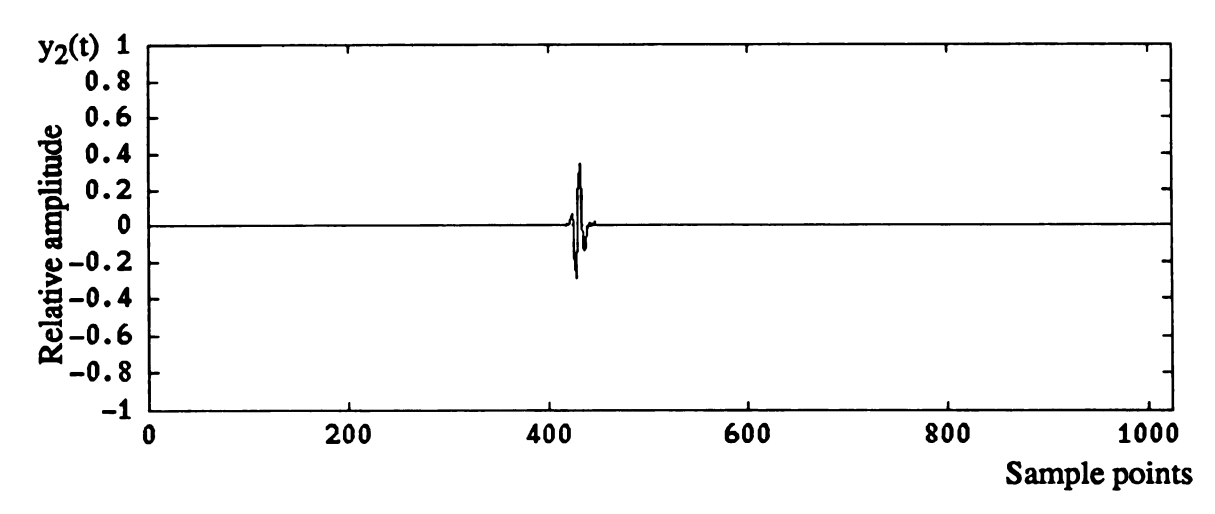


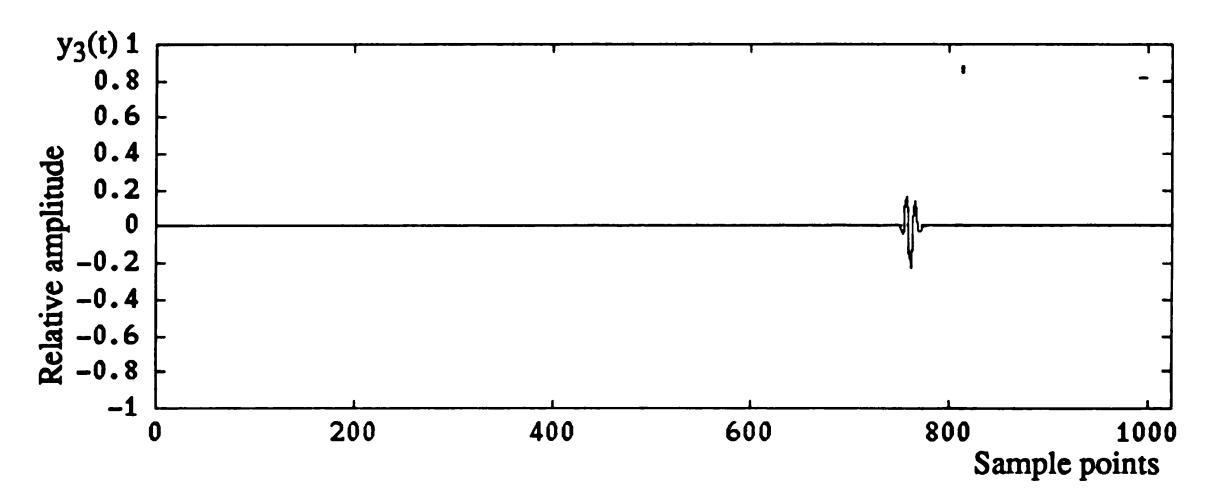
Figure V.12 Measured sequence of gated pulses by variable windows.



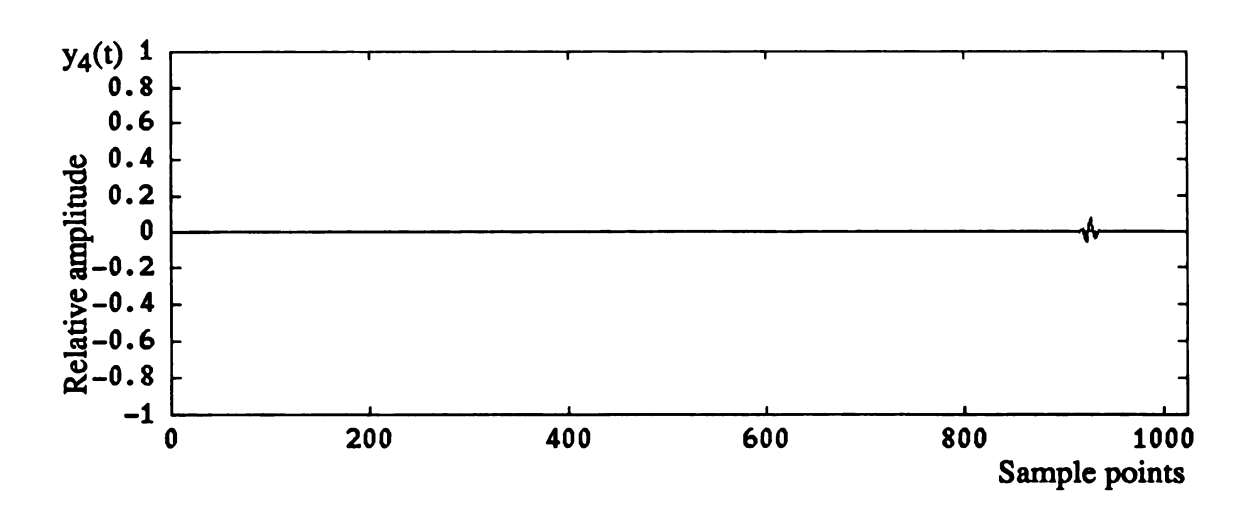
(a) The signal returned from the first boundary was zero padded to 1024-point.



(b) The signal returned from the second boundary was zero padded to 1024-points Figure V. 13 Zero padding of the gated pulses to generate 1024-point signals.



(c) The signal returned from the third boundary was zero padded to be 1024-points.



(d) The signal returned from the fourth boundary was zero padded to be 1024-points.

Figure V.13 (continued)

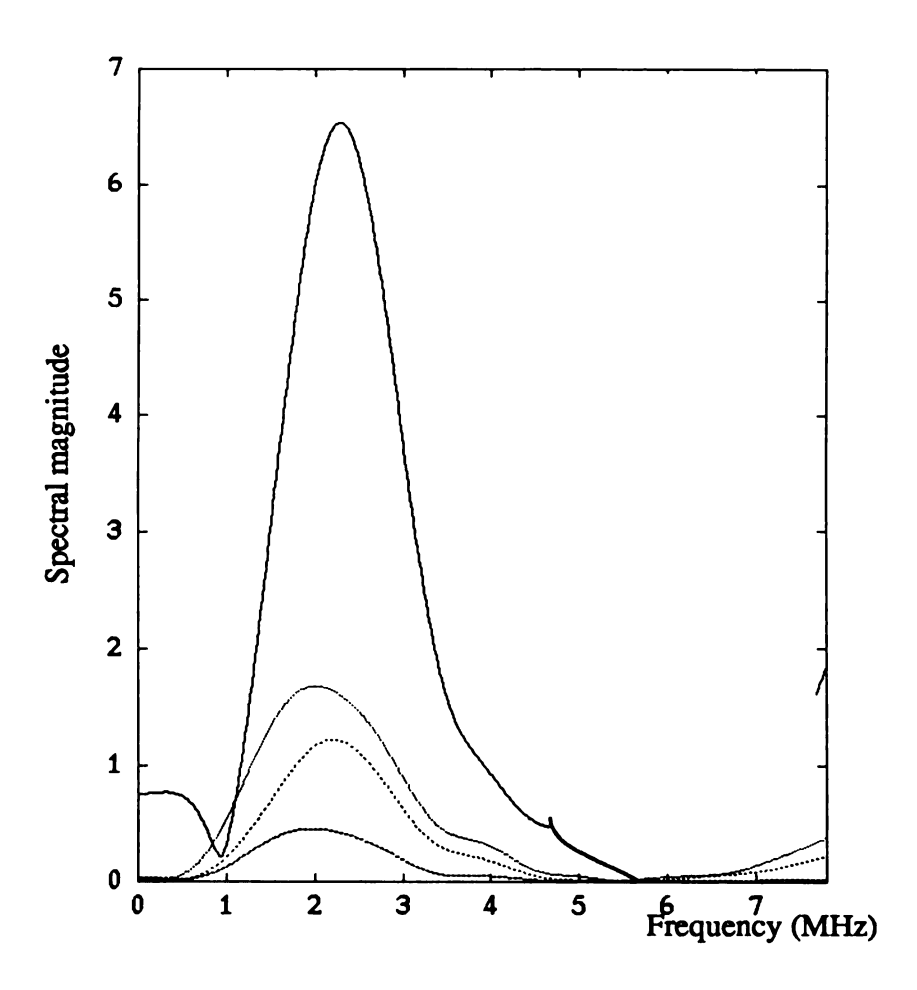


Figure V.14 The spectral magnitudes of the gated pulses on a linear scale.

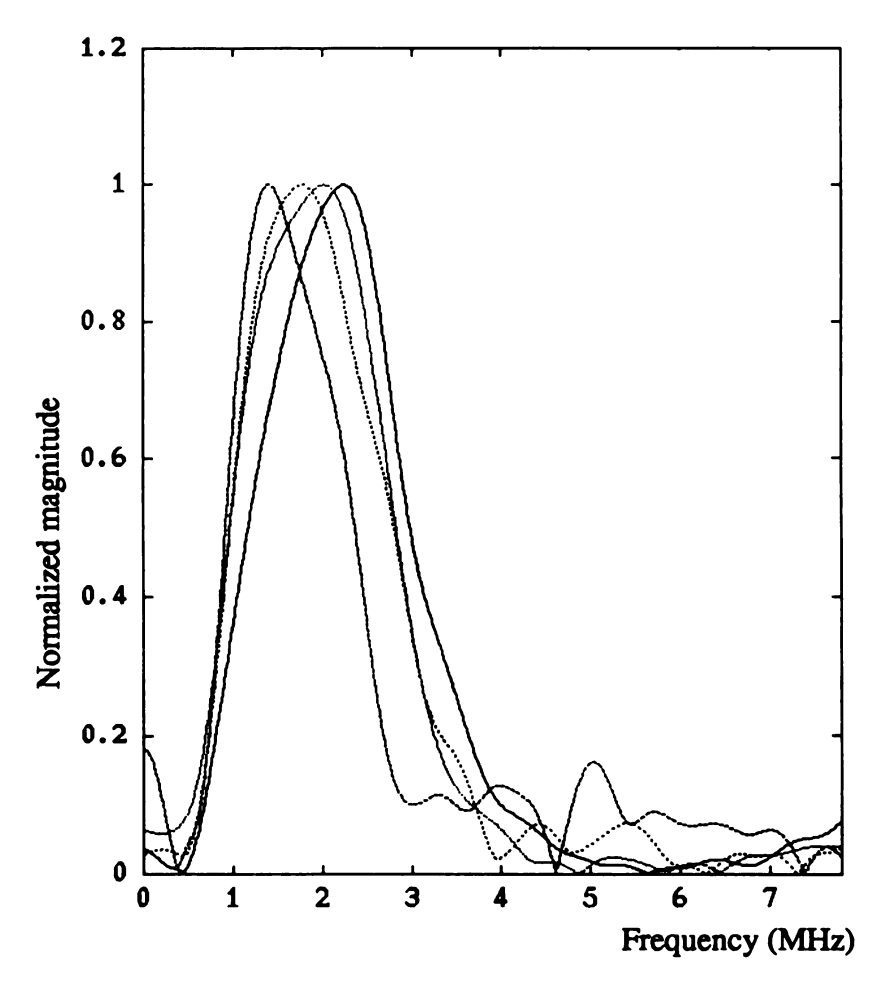


Figure V. 15 Normalized spectral magnitudes of the gated pulses on a linear scale.

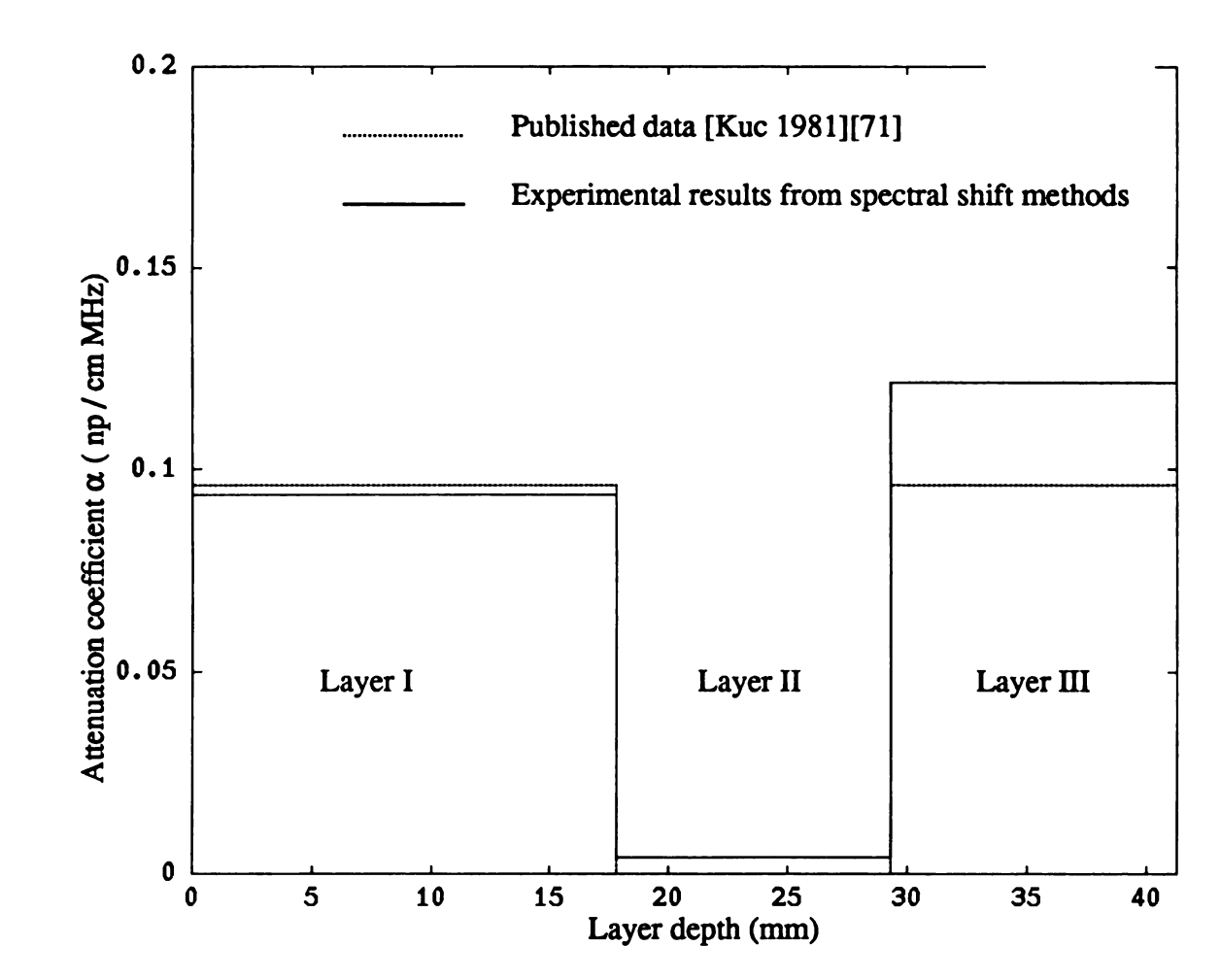


Figure V.16 Attenuation coefficient profiles of multi-layered model obtained by spectral shift techniques.

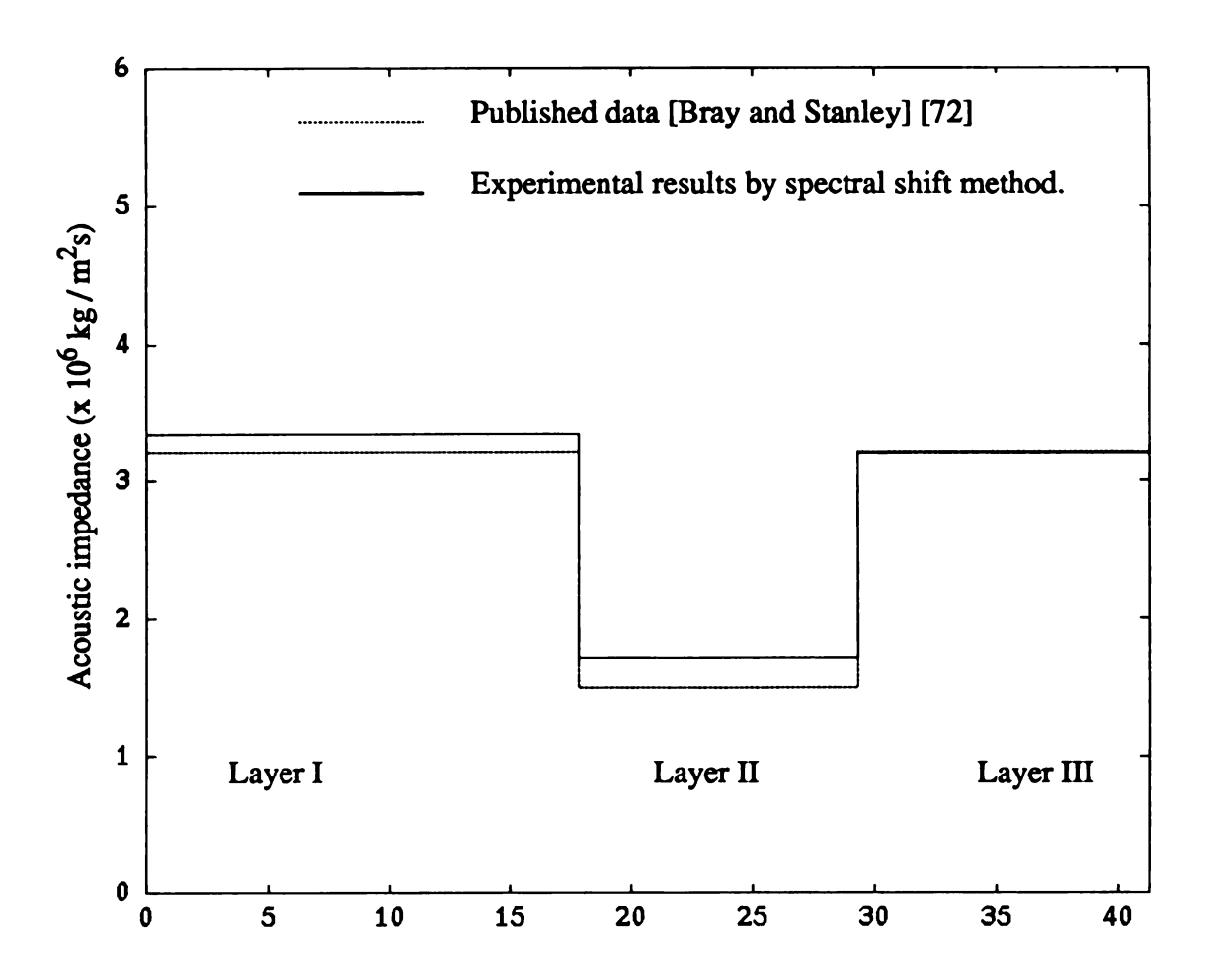


Figure V.17 Acoustic impedance profiles of multi-layered model obtained by spectral shift techniques.

# **CHAPTER VI**

# SUMMARY AND CONCLUSIONS

## VI.1 Limitations and advantages of the proposed time domain method.

It has been shown that the time domain method proposed in this dissertation provides a simple way to evaluate the properties (attenuation coefficients and acoustic impedances) of multi-layered materials. The required experimental data for material characterization are merely the locations and the amplitudes of the echo return from each boundary. Since the time domain process employs the two sided interrogation configuration, this technique can determine not only acoustic impedance but also attenuation coefficients. The technique presented in this dissertation can overcome the common drawbacks of conventional approaches. In particular, the drawbacks considered are: (I) A single-sided pulse-echo interrogation cannot provide the attenuation coefficient and acoustic impedance simultaneously. One of the two quantities (attenuation coefficient or acoustic impedance) must be assumed known, or can be neglected, to obtain the other quantity. (II) A transmission measurement can only provide the accumulated attenuation rather than the

individual attenuation of a multi-layered target.

From the experimental results, the propagation velocities of waves in each layer agree favorably with the reference values. Furthermore, it can be seen that the locations of the boundaries can be accurately determined from an envelope peak detection algorithm. The values of acoustic impedances of each layer agree well with the reference values. Since three separated layers are of the same material in the experimental model, the respective values for those attenuation coefficients are found to be approximately the same, as expected. From the experimental measurement, it was found that the deeper layers have a greater deviation from the reference value than that of the shallower layer. We suspect that the deviations are due to the following:

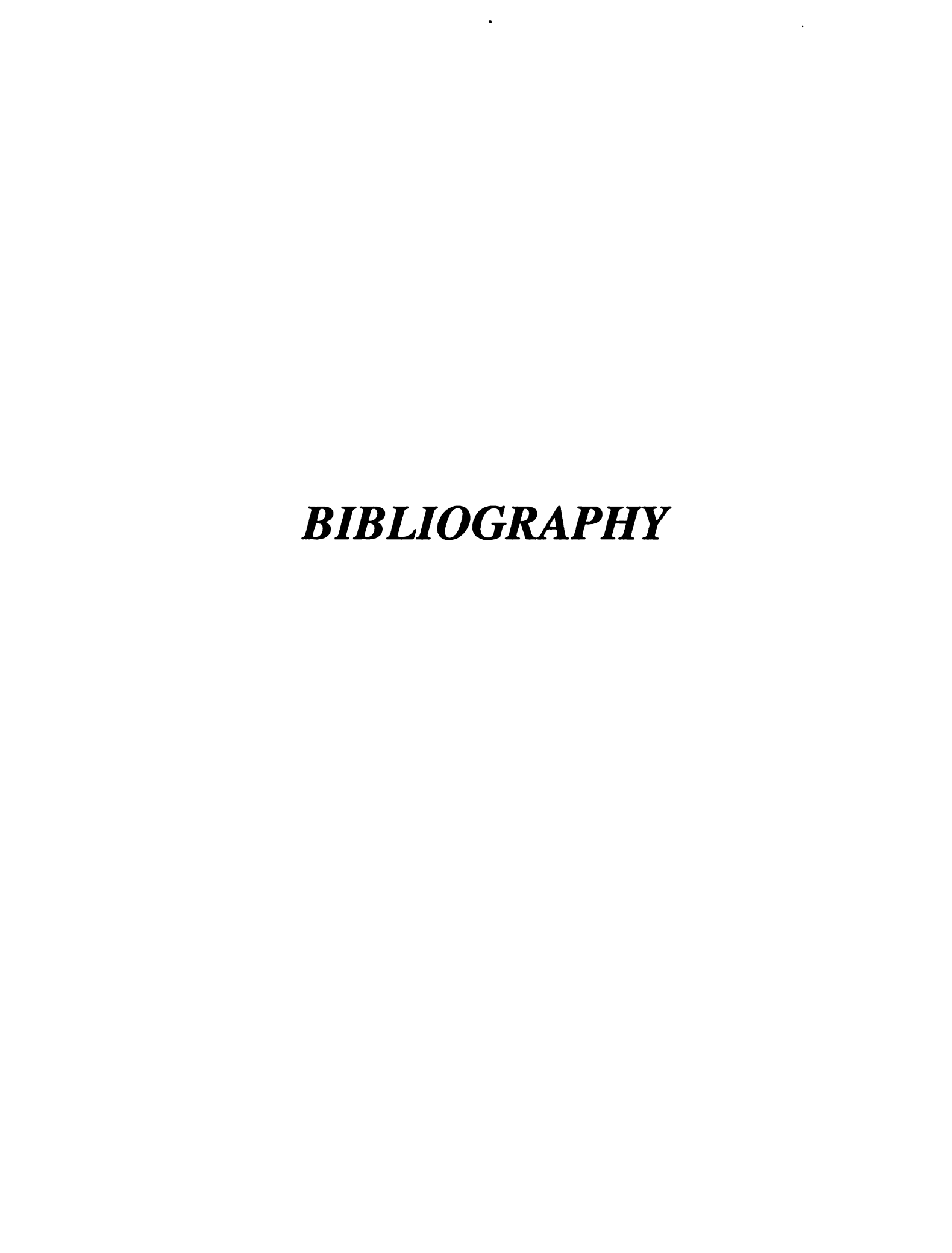
- (1.) The incident wave is not a truly narrow-band signal, as was shown in Figure III.4, and the attenuation coefficients are not totally frequency independent. Consequently, the longer the path of propagation, the greater the wave distortion.
- (2.) In the developed algorithm, the reflection coefficient r<sub>1</sub> at the first boundary is assumed to be accurately known. In practice, this value must be obtained from experimental data. So that if this value is not accurately determined, additional error will accumulate in the deeper layers.
- (3.) Since eight-bit A / D conversion is used for signal acquisition, quantization error will occur for weak signals from the deeper layers.

As has been mentioned, the time domain technique developed in this dissertation has limitations. Nevertheless, it offers a simple way to achieve acceptable results from multi-layered structures. Moreover, it provides an excellent possibility for real-time imaging because of its short processing time.

### VI.2 Limitations and advantages of the proposed spectral shift method.

The proposed spectral shift method discussed in this thesis provides a novel way to evaluate the properties (both attenuation coefficient and acoustic impedance) of multi-layered material. In particular, material for which attenuation can be characterized by either a linear or a quadratic frequency dependency, the frequency shift can be analytically and experimentally validated. It is noteworthy that the technique does not require the information of reflection coefficient or transmittance coefficient to evaluate the attenuation. We were able to determine both the attenuation coefficients and the reflection coefficients (i.e. acoustic impedances) by a single sided interrogation configuration, which is a simpler measurement to perform. However, the technique requires that the incident signals have a Gaussian-shaped spectrum. In practice, it is very difficult to generate a signal with a perfect Gaussian-shaped spectrum. From the experimental results, it was shown that the attenuation coefficient of 0.0935 np cm<sup>-1</sup> MHz<sup>-1</sup>, of the first layer plexiglass sample agrees favorably with Kuc's experimental value of 0.096 np cm<sup>-1</sup> MHz<sup>-1</sup> [72]. For the model used, the first and third layer are made of the same plexiglass material and provided similar values for the attenuation, as expected. The attenuation coefficient for the third layer deviated from the expected values. The deviation of the third layer relative to the first layer is due to the lower signal levels reflected from the deeper sample layer and the quantization error from the eight-bit A / D converter. These factors tended to distort the Gaussian spectrum. For the second layer, which is water, the attenuation coefficient is only 0.00172 np cm<sup>-1</sup> MHz<sup>-2</sup>. For example, an incident wave at 2.25 MHz propagating through 5 cm of water will be attenuated by only 4%. Thus, the assumption of no attenuation for the coupling medium (2~3 cm water) is reasonable. Once the attenuation coefficients for each layer are determined, the acoustic impedances for successive layers can be calculated. From the experimental results, the measured data agree favorably with the published values.

In summary, the mathematical development for multi-layered attenuation coefficients and acoustic impedances, supported by experimental measurements, provides a highly promising technique for material property specification. Applications to composite material evaluation and inspection of alloys appear to be feasible.



# **BIBLIOGRAPHY**

- [1] J. W. Mimbs, M. O'Donnell, J. G. Miller and B. E. Sobel, "Changes in ultrasonic attenuation indicative of early myocardium ischomic injury," *American Journal of Physiol*ogy, vol. 236, pp. 340-344, 1979.
- [2] K. A. Dines and A. C. Kak, "Ultrasonic attenuation tomography of soft tissue," *Ultrasonic Imaging*, vol. 1, no. 1, pp.16-33, 1979.
- [3] J. F. Greenleaf and R. Bahn, "Clinical imaging with transmissive ultrasonic computerized tomography," *IEEE Transactions on Biomedical Engineering*, vol. BME-28, no.2, pp. 177-185, February, 1981.
- [4] J. F. Greenleaf, S. A. Johnson, R. C. Bahn and B. Rajagopalan, "Qantitative cross-sectional imaging of ultrasound parameters," *IEEE Ultrasonics Symposium*, pp. 989-995, 1977.
- [5] J. F. Greenleaf, J. Ylitalo and J. J. Gisvold, "Ultrasonic computed tomography for breast examination," *IEEE Engineering in Medicine and Biology magazine*, pp. 27-32, December, 1987.
- [6] P. L. Carson, C. R. Mair, A. L. Scharzinger and T. U. E. Oughton, "Breast imaging in coronal planes with simulation pulse echo and transmission ultrasound" *Science*, 214, pp. 1141-1143, 1981.
- [7] R. Kuc, M. Schwartz and L. V. Micsky, "Parameter estimation of the acoustic attenuation coefficient slope for soft tissue," *IEEE Ultrasonic Symposium*, pp. 44-47, 1976.
- [8] R. Kuc and M. Schwartz, "Estimating the acoustic attenuation coefficient slope for liver from reflected ultrasound signals," *IEEE Transactions on Sonics and Ultrasonics*, Vol. SU-26, pp. 353-362, 1979.
- [9] R. Kuc, "Clinical application of an ultrasound attenuation coefficient estimation technique for liver pathology characterization," *IEEE Transactions on Biomedical*

## Engineering, Vol. BME-27, pp. 312-317, 1980.

- [10] R. Kuc, "Estimation acoustic attenuation from reflected ultrasonic signal: Comparison of spectral-shift and spectral difference approaches," *IEEE. Transactions on Acoustic, Speech and Signal Processing*, vol. ASSP-32, no.1, pp. 1-6, February, 1984.
- [11] P. He, "A new time domain method for estimating acoustic attenuation of soft tissue," *IEEE Engineering in Medicine & Biology Society 10- th Annual International Conference*, pp. 1122-1123, 1988.
- [12] P. He and J. F. Greenleaf, "Application of stochastic analysis to ultrasonic echoes-Estimation of attenuation and tissue heterogeneity from peaks of echo envelope," J. Acoust. Soc. Am. 79(2), pp. 526-534, February, 1986.
- [13] P. He, "On the estimation of acoustic attenuation coefficient from peak of echo envelope," J. Acoust. Soc. Am. 83(5), pp. 1919-1925, 1988.
- [14] T. Chen, B. Ho and R. Zapp, "Evaluation of tissue attenuation property by bi-directional pulse echo interrogation technique," Fifteen International Symposium on Ultrasonic Imaging and Tissue Characterization, Washington DC, June 11-13, 1990.
- [15] T. Chen and B. Ho, "Nondestructive evaluation of attenuation and speed of ultrasonic wave propagation in layered materials," *American Society for Composite 5th Technical Conference*, East Lansing, Michigan, June 1990.
- [16] P. He, "Acoustic attenuation estimation for soft tissue from ultrasound echo envelope peaks," *IEEE Transactions on Ultrasonics, Ferroelectrics and Frequency Control.* Vol. 36, No. 2, pp. 197-203,1989.
- [17] N. M. Bilgutay and J. Saniie, "The effect of grain size on flaw visibility enhancement using split spectrum processing," *Material Evaluation* 42, pp. 808-814,1984.
- [18] P. M. Shankar, U. Bencharit, N. M. Bilgutay and J. S. Saniie "Grain noise suppression through bandpass filter" *Material evaluation* 46, pp. 1100-1104, July, 1988.
- [19] P. Karpur, P. M. Shankar, J. L. Rose and V. L. Newhouse, "Split spectrum processing: determination of available bandwidth for spectral splitting," *Ultrasonics* vol. 26, pp. 204-209, July, 1988.

- [20] J. D. Aussel, "Split spectrum processing with finite impulse response filters of constant frequency-to-bandwidth ratios" *Ultrasonics*, pp. 630-641, July, 1990.
- [21] J. L. Rose, P. Karpur and V. L. Newhouse, "Utility of split spectrum processing in ultrasonic nondestructive evaluation" *Material Evaluation* 46, pp. 14-22, January, 1988.
- [22] S. M. Gehlbach and F. G. Somme, "Frequency diversity speckle processing," *Ultrasonic Imaging*, vol. 9, pp. 92-105,1987.
- [23] V. L. Newhouse, N. M. Bilgutay, J. Sanile and E. S. Furgasn, "Flaw-to-grain echo enhancement by split spectrum processing," *Ultrasonics*, pp. 59-68, March 1982.
- [24] W. Kohl and R. Schwarz, "A simple method of realizing the deconvolution of ultrasonic images," *Ultrasonics*, pp. 273-278, November, 1981.
- [25] R. N. Carpenter and P. R. Stepanishen, "An improvement in the range resolution of ultrasonic pulse echo systems by deconvolution," *J. Acoust. Soc. Am.* 75(4), pp. 1084-1091, April, 1984.
- [26] G. Hayward and J. E. Lewis, "Comparison of some non-adaptive deconvolution techniques for resolution enhancement of ultrasonic data," Ultrasonics, vol. 27, pp. 155-164, May, 1989.
- [27] E. E. Hundt, and E. Atrautenberg, "Digital processing of ultrasonic data by deconvolution," *IEEE Transactions on Sonics and Ultrasonics*, vol. SU-27, no. 5, pp. 249-252, Sept. 1980.
- [28] C. N. Liu, M. Fatemi, and R. C. Waag, "Digital processing for improvement of ultrasonic abdominal images," *IEEE Transactions. on Medical Imaging*, vol. MI-2, No. 2, pp. 66-75, June, 1983.
- [29] W. Vollmann "Resolution enhancement of ultrasonic B-scan images by deconvolution" *IEEE Transactions on Sonics and Ultrasonics*, vol. SU-29, no.2, pp.78-83, March, 1982.
- [30] J. P. Jones, "Ultrasonic impediography and its application to tissue characterization," Recent Advances in Ultrasound in Biomedicine, pp. 131-154, 1979.

- [31] P. Cobo-Parra and C. Ranz-Guerra, "Impedance profile and overall attenuation of layered sea bottom from their normal incident acoustic reflection response," J. Acoust. Soc. Am. 85 (6), pp. 2388-2393, June 1989.
- [32] G. Kossoff, E. K. Fry and J. Jellins, "Average velocity of ultrasound in the human female breast," J. Acoust. Soc. Am., vol. 53, pp. 1730-1736, 1973.
- [33] G. H. Glover and J. C. Sharp, "Reconstruction of ultrasound propagation speed distribution in soft tissue: time-of-flight tomography," *IEEE Transactions on Sonics and Ultrasonics*, vol. SU-24, no. 4, pp. 229-234, July, 1977.
- [34] T. Pialucha, C. C. H. Guyott and P. Cawlew, "Amplitude spectrum method for the measurement of phase velocity," *Ultrasonics*, vol. 27, pp. 270-279, September, 1989.
- [35] S. I. Rokhlin, D. K. Lewis, K. F. Graff and L. Adler, "Real time study of frequency dependent of attenuation and velocity of ultrasonic transducer," *J. Acoust. Soc. Am.* 79(6), pp. 1783-1793, June 1986.
- [36] M. V. Zummeren, D. Young, C. Habeger, G. Baum and R. Treleven, "Automatic determination of ultrasound velocities in planar materials," *Ultrasonics*, vol. 25, pp.288-294, September, 1987.
- [37] J. Ophir and T. Lin, "A calibration-free method for measurement of sound speed in biological tissue samples," *IEEE Trans. on Ultrasonics, Ferroelectrics, and Frequency Control*, vol. 35, No. 5, pp. 573-577, September, 1988.
- [38] J. Ophir and Y. Yazdi, "A transaxial compression technique for localized pulse echo estimation of sound speed in biological tissue," *Ultrasonic Imaging* 12, pp. 35-46, 1990.
- [39] N. Hayashi et al., "A new method of measuring in vivo sound speed in reflection mode," Journal of Clinical Ultrasound 16, pp.87-93, 1988.
- [40] D. E. Robison, F. Chen and L. S. Wilson, "Measurement of velocity propagation from ultrasonic pulse echo data," *Ultrasound Med. and Biol.* vol. 8, pp. 413-420,1982.
- [41] T. Kontonassios and J. Ophir, "Variance reduction of speed of sound estimation in tissue using the beam tracking method," *IEEE Trans. on Ultrasonics, Ferroelectrics, and Frequency Control*, vol. UFFC-34, no. 5, pp.524-530, September, 1987.

- [42] T. Lin, J. Ophir, and G. D. Potter, "Correlation of sound speed with tissue constituents in normal and diffuse liver disease," *Ultrasonic Imaging*, vol. 9, pp.29-40,1987.
- [43] L. M. Brekhovskikh, ed., "Waves in Layered media,", Second edition, Chapter 3, Academic press, New York, pp. 10-28,1980.
- [44] B. Ho, A. Jayasumana and C. G. Fang, "Ultrasonic attenuation tomography by dual reflection techniques," *IEEE Ultrasonics Symposium*, pp. 770-772, 1983.
- [45] T. Chen, B. Ho and R. Zapp, "Impedance and attenuation profile estimation of multilayered material from reflected ultrasound" to appear in the issue August, 1991, of IEEE Transactions on Instrumentation and Measurement.
- [46] A. C. Kak and K. A. Dines, "Signal processing of broadband pulsed ultrasound: Measurement of attenuation of soft biological tissue," *IEEE Trans. on Biomedical Engineering*, vol. BME-25, no. 4, pp. 321-343, July 1978.
- [47] S. Serabian, "Influence of attenuation upon the frequency content of a stress wave packet in graphite," J. Acoust. Soc. Am. 42, pp. 1052-1059, 1967.
- [48] S. W. Flax, N. J. Pele, G. H. Glover, F. D. Gutmann, and M. Mclachlan, "Spectral characterization and attenuation measurement in ultrasound," *Ultrasonic Imaging* 5, pp. 95-116, 1983.
- [49] P. A. Narayana, J. Ophir, "Spectral shifts of ultrasonic propagation: a study of theoretical and experimental models," *Ultrasonic Imaging* 5, pp.22-29, 1983.
- [50] W. H. Round and R. H. T. Bates," Modification of spectra of pulses from ultrasonic transducer by scatters in non-attenuating and in attenuating media," Ultrasonic Imaging 9, pp. 18-28, 1987.
- [51] J. Ophir and P. Jaeger, "Spectral shift of ultrasonic propagation through media with nonlinear dispersive attenuation," *Ultrasonic Imaging* 4, pp. 282-289, 1982.
- [52] M. Insana, J. Zagzebski and E. Madsen, "Improvement in the spectral difference method for measuring ultrasonic attenuation" *Ultrasonic Imaging* 5, pp.331-345, 1983.
- [53] Y. Hayakawa *et al.*, "Measurement of ultrasound attenuation coefficient by a multi-frequency echo technique theory and basic experiment," *IEEE Trans. on Ultra*-

- sonic, Ferroelectrics and Frequency Control, vol. UFFC-33, no. 6, pp.759-764, Nov. 1986.
- [54] T. Chen, B. Ho and R. Zapp, "Evaluation of multi-layered material properties by spectral shift acoustic reflectometry," *In preparation*.
- [55] W. J. Fry and F. Dunn, "Ultrasound: Analysis and Experimental method in Biological research," *In Physical Technique in Biological Research*, vol.4, Academic press, New York, pp. 261-314, 1962.
- [56] E. L. Madsen, H. J. Satkoff and J. A. Zagzebski, "Ultrasonic shear wave properties of soft tissue and tissuelike material," J. Acoust. Soc. Am. 74, pp.1346-1355,1983.
- [57] H. Pauly and H. P. Schwan, "Mechanism of absorption of ultrasound in liver tissue," J. Acoust. Soc. Am 50(2), pp. 692-699, 1971.
- [58] J. Ophir, R. E. McWhirt, N. F. Maklad, and P. M. Jaeger, "A narrow band pulse-echo technique for *in vivo* ultrasonic attenuation estimation," *IEEE Trans. on Biomedical Engineering*, vol. BME-32, no. 3, pp. 205-212, March, 1985.
- [59] J. Nodar, "Determination of atteuation-velocity product of homogeneour layered media," Ph. D Dissertation, Michigan State University, 1989.
- [60] J. G. Proakis and D. G. Manolakis, "Introduction to digital signal processing," Mcmillan publishing company, New York, pp. 230, 1988.
- [61] R. Kuc, "Bounds on estimating the acoustic attenuation of small tissue region from reflected ultrasound," *Proceeding of IEEE*, vol. 73, no.7, July, 1985.
- [62] L. S. Wilson, D. E. Robinson and B. D. Doust, "Frequency domain processing for ultrasonic attenuation measurement in liver," *Ultrasonic Imaging* 6, pp.278-292, 1984.
- [63] S. O. Rice, "Mathematical analysis of random noise," *Bell System Technical Journal*, 23, pp. 282-332, 1944.
- [64] Papoulis, "Probability, random variable and stochastic process," McGraw Hill, New York, pp. 485,349, 1965.
- [65] J. Ophir, M. A. Ghouse and L. A. Ferrari, "Attenuation estimation with zero-crossing technique: Phantom studies," *Ultrasonic Imaging* 7, pp. 122-132,1985.

- [66] S. W. Flax, N. J. Pelc, G. H. Glover, F. D. Gutman and M. McLanclian, "Spectral characterization and attenuation measurement in ultrasound," *Ultrasonic Imaging* 5, pp. 95-116, 1983.
- [67] P. A. Nayayana and J. Ophir, "On the frequency dependent of attenuation in normal and fatty liver," *IEEE Trans. on Sonics and Ultrasonics*, vol. SU-30, No.6, pp.379-383, 1983.
- [68] S. Shaffer, D. W. Pettibone, J. F. Havlice and M. Nassi, "Estimation of the slope of the acoustic attenuation coefficient," *Ultrasonic Imaging*, 6, pp. 126-138, 1984.
- [69] P. He and A.McGoron, "Parameter estimation for nonlinear frequency dependent attenuation in soft tissue," *Ultrasound in Medical & biology*, vol. 15, no. 8. pp757-763,1989.
- [70] P. A. Narayana and J. Ophir, "A Closed Form Method for the Measurement of Attenuation in Nonlinear Dispersive Media," *Ultrasonic Imaging*, vol. 5. pp.17-21,1983.
- [71] P. A. Narayana, J. Ophir and N. F. Maklad, "The Attenuation of Ultrasound in Biological Fluid," J. Acoust. Soc. Am. 76(1), pp. 1-4, July, 1984.
- [72] R. Kuc, "Digital filter model for media having linear with frequency loss characteristics," J. Acoust. Soc. Am. 69 (1), pp. 35-40, Jan. 1981.
- [73] D. E. Bray and R. K. Stanley, "Nondestructive evaluation: A tool for design and manufacturing, and service," McGraw-Hill serial in Mechanical Engineering, pp. 53, New York, 1989.